# Chapter 13
# Atmospheric Dynamics and Meteorology

F. M. Flasar, K. H. Baines, M. K. Bird, T. Tokano, and R. A. West

**Abstract** Titan, after Venus, is the second example in the solar system of an atmosphere with a global cyclostrophic circulation, but in this case a circulation that has a strong seasonal modulation in the middle atmosphere. Direct measurement of Titan's winds, particularly observations tracking the Huygens probe at 10°S, indicate that the zonal winds are mostly in the sense of the satellite's rotation. They generally increase with altitude and become cyclostrophic near 35 km above the surface. An exception to this is a sharp minimum centered near 75 km, where the wind velocity decreases to nearly zero. Zonal winds derived from temperatures retrieved from Cassini orbiter measurements, using the thermal wind equation, indicate a strong winter circumpolar vortex, with maximum winds of 190 m $s^{-1}$ at mid northern latitudes near 300 km. Above this level, the vortex decays. Curiously, the stratospheric zonal winds and temperatures in both hemispheres are symmetric about a pole that is offset from the surface pole by ~4°. The cause of this is not well understood, but it may reflect the response of a cyclostrophic circulation to the offset between the equator, where the distance to the rotation axis is greatest, and the seasonally varying subsolar latitude. The mean meridional circulation can be inferred from the temperature field and the meridional distribution of organic molecules and condensates and hazes. Both the warm temperatures near 400 km and the enhanced concentration of several organic molecules suggest subsidence in the north-polar region during winter and early spring. Stratospheric condensates are localized at high northern latitudes, with a sharp cut-off near 50°N. Titan's winter polar vortex appears to share many of the same characteristics of isolating high and low-latitude air masses as do the winter polar vortices on Earth that envelop the ozone holes. Global mapping of temperatures, winds, and composition in the troposphere, by contrast, is incomplete. The few suitable discrete clouds that have been found for tracking indicate smaller velocities than aloft, consistent with the *Huygens* measurements. Along the descent trajectory, the Huygens measurements indicate eastward zonal winds down to 7 km, where they shift westward, and then eastward again below 1 km down to the surface. The low-latitude dune fields seen in Cassini RADAR images have been interpreted as longitudinal dunes occurring in a mean eastward zonal wind. This is not like Earth, where the low-latitude winds are westward above the surface. Because the net zonal-mean time-averaged torque exerted by the surface on the atmosphere should vanish, there must be westward flow over part of the surface; the question is where and when. The meridional contrast in tropospheric temperatures, deduced from radio occultations at low, mid, and high latitudes, is small, ~5 K at the tropopause and ~3 K at the surface. This implies efficient heat transport, probably by axisymmetric meridional circulations. The effect of the methane "hydrological" cycle on the atmospheric circulation is not well constrained by existing measurements. Understanding the nature of the surface-atmosphere coupling will be critical to elucidating the atmospheric transports of momentum, heat, and volatiles.

Uncorrected Proof

## 13.1 Introduction

Planetary atmospheres are nonlinear dynamical systems that resist easy analysis or prediction. While theoretical studies ranging from "simple" scaling to general circulation models (GCMs) are critical tools for developing a conceptual understanding of how an atmosphere works, these must be closely tethered to observations. The range of possibilities is too rich and complex to do otherwise. The study of extraterrestrial planetary atmospheres has traditionally drawn on the much richer body of work on the terrestrial atmosphere, but Earth is only one realization. Much of the excitement in studying planetary atmospheres is to avail oneself of the large-scale natural

F.M. Flasar (✉)
NASA Goddard Space Flight Center
e-mail: f.m.flasar@nasa.gov

K.H. Baines and R.A. West
California Institute of Technology, Jet Propulsion Laboratory

M.K. Bird
Universität Bonn

T. Tokano
Universität zu Köln

R. Brown et al. (eds.), *Titan from Cassini-Huygens*,
© Springer Science+Business Media B.V. 2009



ch13.indd 323 7/22/2009 7:59:01 PM

laboratories that other worlds provide and examine the response of atmospheres to different sets of external factors (e.g., surface or internal rotation, solar forcing, internal heat fluxes). Trying to reconcile the observed behavior of atmospheres to different forcing factors is an important step to achieving a deeper insight into the physical processes that govern it.

In the mix of available natural planetary laboratories, Saturn's giant moon Titan offers an intriguing blend. In several aspects, it resembles Earth. Its atmosphere is primarily $N_2$, and its surface pressure is about 50% larger than Earth's. After $N_2$, the most abundant constituent is not $O_2$ but $CH_4$. Photo- and electron-impact dissociation of $CH_4$ and $N_2$ leads to the irreversible production of more complex organic molecules that either condense and precipitate or else form the photochemical smog that enshrouds Titan. There is evidence for an analog to a hydrological cycle in Titan's troposphere, involving $CH_4$, not $H_2O$. Its middle atmosphere (i.e., stratosphere and mesosphere) has strong circumpolar winds in winter, with cold polar temperature, condensate ices, and anomalous concentrations of several gases. This is reminiscent of the ozone holes on Earth. There are differences, too. Titan is much colder than Earth, and the radioative response of its atmosphere is much longer. For this reason, thermal tides probably do not play an important role in Titan's lower and middle atmosphere, but gravitational tides may, induced by Titan's eccentric orbit about Saturn. Titan is a much slower rotator than Earth: its "day" is 15.95 terrestrial days. In this regard, it is more like Venus, another slow rotator, and it provides the second example of an atmosphere with a global cyclostrophic wind system, i.e., the atmospheric winds whip around the body in much less time that it takes the surface to rotate by 360°.

This chapter reviews the dynamic meteorology of Titan's lower and middle atmosphere, i.e., its troposphere, stratosphere, and mesosphere (Fig. 13.1), particularly drawing on the Cassini-Huygens data that have been acquired and analyzed to date. Section 13.2 briefly reviews the radiative and dynamical time-scales in Titan's atmosphere. Section 13.3 discusses Titan's temperatures and zonal winds, derived from Voyager, ground-based, and Cassini-Huygens measurements. The zonally averaged temperatures and mean zonal winds are coupled by the thermal wind equation. Meridional winds (Section 13.4) can be inferred more indirectly from the temperature field, as well as from quasi-conserved tracer gases and from the distribution of condensates; the Huygens probe also provided in situ measurements at 10°S. Section 13.5 focuses on the energy and momentum exchange between the surface and atmosphere and the structure of Titan's planetary boundary layer. Atmospheric waves, particularly gravitational tides, are the subject of Section 13.6. They are of interest because they can transport zonal momentum over large distances and, because their horizontal and vertical propagation depends on the thermal stability and

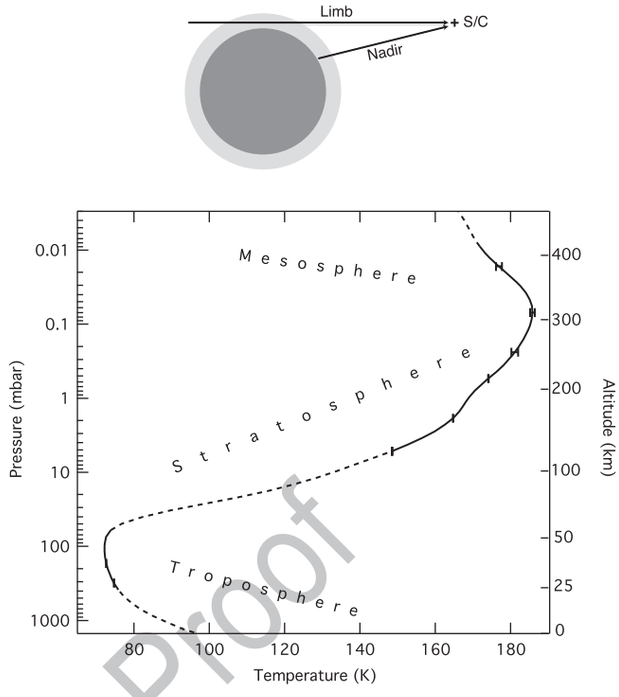


**Fig. 13.1** Vertical profile of temperature at 15°S from Cassini CIRS mid- and far-infrared spectra obtained during northern winter. The *solid portions* of the profile indicate altitudes where the spectra constrain the temperature retrieval. The *upper portion* is from the spectral region of the $\nu_4$ band of $CH_4$ at 7.7 μm, using both nadir- and limb-viewing geometry (illustrated at top; nadir viewing denotes the situation in which the line of sight intersects the surface); the *lower portion* is from far-infrared spectra near 100 μm, where pressure-induced $N_2$ absorption dominates, using only nadir-viewing geometry. The *dashed portions* of the profile are not well constrained by the spectra and are essentially initial guesses, based on temperatures retrieved from the Voyager radio occultations (after Flasar et al. 2005)

wind structure of the mean atmosphere, they are also useful probes of atmospheric structure. Section 13.7 summarizes the current understanding of Titan's general circulation, both conceptually and by the success of GCMs in simulating Titan's atmospheric behavior. Finally Section 13.8 concludes by summarizing key questions concerning Titan's meteorology and near-term prospects for addressing them. Earlier reviews of Titan's dynamic meteorology that may be of interest can be found in Hunten et al. (1984), Flasar (1998a, b), Flasar and Achterberg (2008), and Tokano (2008b). [AU1]

## 13.2 Radiative and Dynamical Time Constants

Before discussing measurements of meteorological variables on Titan and their interpretation, it is helpful to briefly discuss the notion of radiative relaxation times and dynamical

Uncorrected Proof

turnover times, which will be used repeatedly in the ensuing discussion.

### 13.2.1 Radiative

Titan's atmosphere is an interesting entity: its radiative response varies by several orders of magnitude as one moves vertically through the atmosphere. The early analysis of Voyager data indicated that Titan's radiative relaxation time – the time over which its temperature relaxes to a radiative equilibrium profile from an initial disturbance, extending over an altitude that is typically on the order of a pressure scale height – was quite large in the troposphere, ~130 years (Smith et al. 1981), and decreased with altitude to a value ~1 year in the upper stratosphere near 1 mbar (Flasar et al. 1981) (see Hunten et al. 1984 and Flasar 1998b for more discussion). More recent radiative flux measurements by the Huygens Probe Descent Imager/Spectral Radiometer (DISR) have indicated a time constant on the order of 500 years in the lower troposphere (Tomasko et al. 2008; Strobel et al. 2009, Ch. 11, Fig. 11.5). Two conclusions follow. The first is that, since the radiative relaxation times in Titan's troposphere and middle atmosphere are much longer than its day (15.95 days) divided by $2\pi$[1], one does not expect solar-driven diurnal effects, e.g., thermal tides, to be very important. The second is that radiative time scales in the upper stratosphere are much smaller than Titan's year (29.5 years) divided by $2\pi$, so there should be a strong response to the seasonal modulation of solar heating. The measurements discussed in the following sections bear this out. Given the very long radiative time constant in the troposphere, Flasar et al. (1981) suggested that seasonal variations there would be very weak. However, this neglected any effects that seasonal variation in surface temperatures would have in coupling to the atmosphere. The heat capacity in the annual skin depth of the surface is much smaller than that corresponding to the lowest scale height of atmosphere (Tokano 2005), particularly in the absence of global oceans or widespread deep lakes. Enough solar radiation (~10%, McKay et al. 1991) makes it through the atmosphere to the surface to produce a seasonal variation in its temperature. Coupling of the surface to the atmosphere through thermally driven convection heats the lower atmosphere seasonally. GCM model simulations generally display a strong seasonal component (Section 13.7). From GCM simulations, Tokano (2005) has concluded that the thermal inertias of some plausible surface materials is low enough that a diurnal variation is possible.

[AU2]

[1]For a harmonic disturbance, the relevant time scale is the period divided by $2\pi$ (see, e.g., Section V of the review by Hunten et al. 1984).

### 13.2.2 Dynamical

For global-scale flow, the dynamical time scale is the turnover time, the horizontal scale of a circulation cell, divided by the horizontal velocity. For the axisymmetric meridional circulations thought to be important on Titan, the horizontal scale is on the order of a planetary radius (Section 13.7). The turnover times can be comparable to a season. When the dynamical time scale is longer than the radiative time scale, there can be an additional, dynamical inertia that acts to retard the atmosphere's relaxation to the radiative equilibrium state. For example, temperatures obtained by the Voyager infrared measurements indicated a north–south asymmetry at 1 mbar (Flasar and Conrath 1990). This was curious, because the Voyager season was shortly after northern equinox, and the radiative relaxation time was relatively short. Bézard et al. (1995) suggested that this might result from a hemispheric asymmetry in the opacities for solar and thermal radiation. Flasar and Conrath (1990) alternatively suggested a dynamical origin. They noted although temperatures could rapidly relax to an equilibrium configuration radiatively, they were coupled to the zonal wind fields by the thermal wind equation (Section 13.3). Hence to reach the equilibrium state angular momentum also had to be transported from the northern hemisphere to the southern. The dynamical turnover time for achieving this transport was comparable to a season on Titan, implying that the stratospheric temperatures and zonal winds would always lag the solar heating, despite the small radiative relaxation time.

## 13.3 Temperatures and Zonal Winds

Any study of atmospheric dynamics and meteorology is predicated on having measurements of temperatures, winds, and gaseous constituents and other tracers of motions in three dimensions. Spatially resolved observations of Titan only began with spatially resolved imaging by Pioneer 11 during its flyby in 1979 (Tomasko and Smith 1982), and in earnest with the Voyager 1 and 2 close passages in 1980 and 1981 a few months after its northern spring equinox. The Cassini orbiter and Huygens probe, observing Titan in northern winter, have provided the best resolution and global coverage to date. Images from the Hubble Space Telescope and imaging using ground-based adaptive optics have provided important information on Titan's state between the two missions, albeit at lower spatial resolution. Finally, much of what we have learned about Titan's zonal winds and their seasonal modulation before Cassini-Huygens has come from Earth-based observations, including stellar occultations, heterodyne spectroscopy, and correlation spectroscopy.

Uncorrected Proof

Temperature, wind, and composition fields are often cast in terms of zonal averages, i.e., averages around a latitude circle. These mean variables define the general circulation, and it is its seasonal and longer-term climatological variations that one seeks to understand. Often the coverage in longitude is not very extensive and surrogate representations must be used, e.g., retrieved variables at a specific longitude or a few longitudes. For instance, spectra from nadir-viewing observations by the Cassini Composite Infrared Spectrometer (CIRS) cover latitude and longitude extensively, and temperatures and composition retrieved from this data can be used to construct true zonal averages. On the other hand, CIRS limb-viewing observations are more sparsely distributed in longitude, and true zonal averages are not possible for these spectra. Fortunately, available evidence, including the CIRS nadir spectra, indicate that zonal variations in temperatures, derived winds, and composition on Titan are usually smaller than meridional variations (see, e.g., Teanby et al. 2008). Hence the ensuing discussion of meteorological variables in this section and the next (Section 13.4) will often be in terms of zonally averaged quantities, even though the measurements themselves have not always provided sufficient data to construct these averages.

### 13.3.1 Temperatures

Chapter 10 (Strobel et al. 2009) discusses the vertical structure of temperature in some detail, so comments here are brief. Figure 13.1 illustrates that the thermal structure of Titan's lower and middle atmosphere, at least at low latitudes, is remarkably reminiscent of Earth's, with a well-defined troposphere, stratosphere, and mesosphere. Titan's temperatures are much lower than Earth's, because of its greater distance form the sun, and the pressure scale height – ranging from 15 to 50 km – is much larger than on Earth (5–8 km), mainly because the gravitational acceleration on Titan–1.3 m $s^{-2}$ at the surface – is much smaller. In fact the large scale height means that Titan's atmosphere is much more extended than most planetary atmospheres in the solar system. The 10 μbar level in the mesosphere, for example, roughly corresponds an altitude of 400 km, a sizeable fraction of Titan's 2,575-km radius. Near-infrared images of Titan from the Visual and Infrared Mapping Spectrometer (VIMS) show methane fluorescence up to ~730 km altitude (Baines et al. 2005).

The vertical profile of temperature is primarily important as a measure of the stability of an atmosphere, i.e., how stable an atmosphere is to vertical motions and whether waves can propagate and how they are refracted by the mean flow when they propagate vertically and horizontally. However, it is the lateral variations in temperature that serve as diagnostics of the departure of an atmosphere from purely radiative response and of the structure of meridional circulations (Section 13.4). Measuring horizontally resolved thermal structure has really only been achieved by the close-up reconnaissances of Voyager and Cassini-Huygens. The ingress and egress of the single Voyager 1 radio-occultation sounding were both in the equatorial region, although at nearly diametrically separated longitudes. Little variation in the troposphere and lower stratosphere was evident (Lindal et al. 1983). The Voyager thermal-infrared spectrometer (IRIS) obtained reasonable latitude coverage during the Voyager 1 flyby, but coverage in longitude was limited to two strips on the day and night sides, nearly 180° apart. Moreover, the IRIS spatial resolution was limited: spectra had to be averaged in latitude bins, typically 15° or larger, in order to obtain an adequate signal-to-noise ratio (Flasar et al. 1981). Only in the upper stratosphere~1 mbar (1 mbar = 1 hPa = 100 Pa) could temperatures be retrieved on isobars, by inverting the observed radiances in the $\nu_4$ band of $CH_4$ near 1.300 $cm^{-1}$ (7.7 μm) and assuming that the gas was uniformly distributed with latitude. Temperatures at high northern latitudes were ~12–20 K colder than at the equator; temperatures in the south were flatter between the equator and 50°, where they began to fall off toward the pole. Neither pole was well observed. Other wavelength regions near 200 $cm^{-1}$ and 530 $cm^{-1}$ probed the tropopause and surface, respectively. Little meridional variation was evident. Temperature variations near the tropopause were ~1 K, and the equator-to-pole contrast at the surface was ~2-3 K. The difficulty was that these differences were estimated from brightness temperatures; the unknown and heterogeneously distributed opacity sources at these wavelengths precluded direct retrieval of temperatures.

Cassini-Huygens, with a more capable array of in situ and remote-sensing instruments, has greatly extended global mapping of atmospheric temperatures at high spatial resolution. For the Cassini spacecraft, this is ensured in no small part by virtue of its being in orbit about Saturn and returning to Titan repeatedly, where its proximity allows good spatial resolution. Preliminary analysis of several radio-occultation soundings at mid and high southern latitudes and high northern latitudes, together with the descent temperature profile from the Huygens Atmospheric Structure Instrument (HASI; see Chapter 10), indicate that the meridional variation of temperatures in the troposphere is small, ~5 K at the tropopause and ~3 K near the surface. Most of the global mapping of atmospheric temperatures is from CIRS thermal-infrared spectra, but these do not permit retrieval of temperatures in the lowest 1½ scale heights (Flasar et al. 2004).

Most of the retrieved temperature maps to date have been from CIRS nadir- and limb-viewing in the mid-infrared, using the observed radiances in the $\nu_4$ band of $CH_4$ as a thermometer to probe the atmosphere above the 10-mbar level.

Uncorrected Proof

This is a classic case of going after the low-lying fruit first. The far-infrared radiances, which include pressure-induced $N_2$ absorption and the rotational lines of $CH_4$, probe lower in the atmosphere and are more affected by aerosol and condensate opacity, which require more careful analysis to retrieve temperatures. Figure 13.2 (top) depicts the meridional cross section of temperatures in Titan's middle atmosphere, retrieved from limb and nadir spectra. The vertical range over which there is information on temperature is 5–3 μbar, except in the colder regions at high northern winter latitudes, where the information content dies away at the 2 mbar level (Achterberg et al. 2008a). Given these caveats, the most dramatic aspect of the temperature field is the behavior at high northern latitudes. Below the 0.1-mbar level, the north polar region is colder than at lower latitudes. This is expected, because it is the region of polar night, and the radiative relaxation time is relatively short (Section 13.2). The temperature contrast is 20–30 K. However, higher up in the stratosphere, the high northern latitudes become the warmest part of Titan's atmosphere, with temperatures

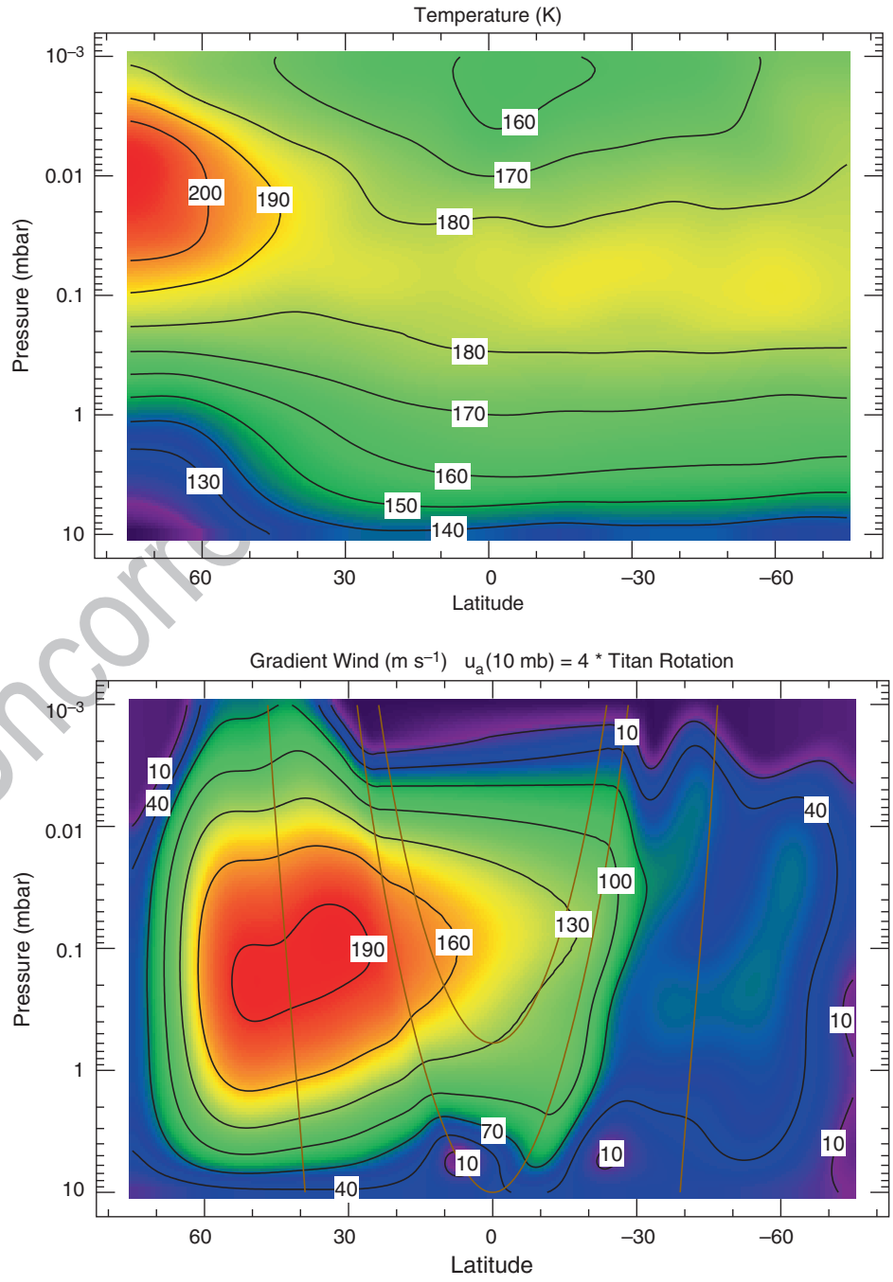


**Fig. 13.2** *Top panel.* Meridional cross section of temperature (K) from CIRS limb and nadir spectra in the mid infrared. *Bottom panel.* Zonal winds (m $s^{-1}$) computed from the thermal wind equation (13.7) with the winds at 10 mbar set to uniform rotation at four times Titan's rotation rate. Positive winds are eastward. The *parabolic curves* correspond to surfaces parallel to Titan's rotation axis (after Achterberg et al. 2008a)

Uncorrected Proof

exceeding 200 K. Titan's polar night does not extend to these higher altitudes. At winter solstice, its north pole is tilted by ~26.7° away from the sun, so the maximum height of shadow, in the absence of atmospheric scattering, is

$$\left(\frac{1}{\cos 26.7^{\circ}} - 1\right) 2575 \approx 307 \text{ km}$$

(~70 μbar). Given the thick condensate hazes that are observed at high northern latitudes during the winter and early spring, it is conceivable that radiative heating may contribute to the warm anomaly observed, but this has not been studied. It may also have a dynamical origin, and this is discussed in Section 13.4.

The figure indicates that the stratopause, the altitude of the maximum temperature marking the boundary between the stratosphere and the mesosphere, varies with latitude. It is lowest near the equator, where it is at the 70-μbar level. It rises slightly toward the south pole, but its elevation increases dramatically toward the north pole,~10 μbar. This is a far greater scale-height variation than seen on Earth (see, e.g., Andrews et al. 1987).

The longitude coverage afforded by CIRS limb soundings is limited, and nadir mapping in the middle infrared has provided most of the information on the zonal structure of temperatures, between 0.5 and 5 mbar. An unexpected result of the mapping was the discovery that the pole of symmetry of the stratospheric temperatures is tilted approximately 4° relative to the IAU definition of the polar axis, which is normal to Titan's orbit about Saturn. The spectral decomposition of the zonal temperature structure relative to the IAU pole indicated a strong wavenumber-1 component (one wavelength around the latitude circle) at most latitudes, and it was strongest at the latitudes having the strongest meridional gradients in temperature. Moreover, the phase of the wavenumber-1 component (i.e., the longitude of the warmest temperatures) remained nearly constant with latitude in each hemisphere, flipping by 180° across the equator. Since both poles are cooler than low latitudes near 1 mbar (Fig. 13.2), this strongly suggested a global tilt of the atmospheric pole of symmetry. By recalculating the zonal variances for an ensemble of new pole positions, the tilt was determined by minimizing the global variance of the temperatures from their zonal means (Achterberg et al. 2008b). Figure 13.3 displays the 1-mbar temperatures; the offset of the axis of symmetry from the IAU pole position is more evident in the northern hemisphere, where the meridional gradients are larger. In the northern hemisphere the tilt of the pole is toward the sun, but about 76°W of the solar direction. The temperatures about the tilted axis are nearly axisymmetric at most latitudes: the standard deviation of the zonal variation is not much greater than that propagating from the CIRS instrument noise. Because of the thermal wind equation, the winds tend to flow along isotherms (see Section 13.3.2.1), and thus are also centered about the offset pole. The 4° tilt is an order of magnitude greater than the recent measurement of the tilt of the rotation pole of the solid surface (Stiles et al. 2008).

Corrected Proof

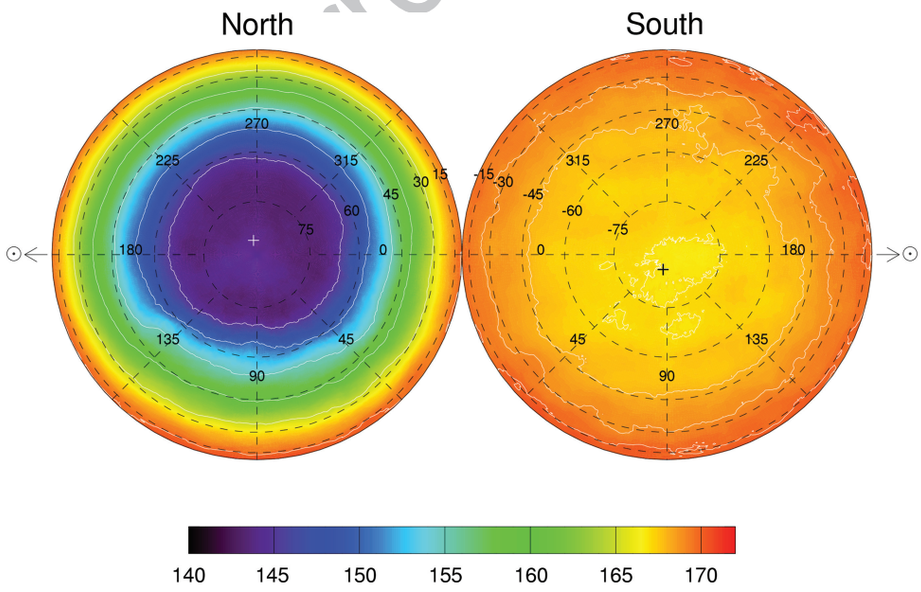


**Fig. 13.3** Polar projection maps of retrieved temperatures at the 1-mbar level. The northern hemisphere is shown on the *left* and the southern hemisphere on the *right*. The color-coded temperature scale in kelvins is shown at the *bottom*. The superposed grid represents latitude and west longitude in a sun-fixed frame with the longitude of the sub-solar point at 180°W, such that the sun direction is towards the left and right edges of the figure. Temperature contours are plotted at intervals of 5 K in the northern hemisphere, and 1 K in the southern hemisphere. The fitted axis of symmetry is indicated by *white* and *black crosses* (+) in the north and south, respectively (after Achterberg et al. 2008b)

### 13.3.2 Zonal Winds

The likely presence of strong zonal winds on Titan had been inferred from infrared observations during the Voyager 1 flyby in November 1980. A distinct pole-to-equator latitudinal contrast in temperature was revealed, varying from $\Delta T \approx 3$ K at the surface to $\Delta T \approx 20$ K in the stratosphere (Flasar et al. 1981). The meridional gradients and the thermal wind equation implied an atmosphere that globally superrotates, analogous to that observed on Venus. To date zonal winds calculated from temperature and pressure fields have provided the most detailed picture of the global wind field. However, these suffer from ambiguities with respect to the wind direction and the need for a (often unknown) boundary condition when the zonal winds are derived from temperatures. Hence direct methods, based on observing the Doppler shifts of molecular lines, tracking discrete clouds, or tracking the descent of the Huygens probe, provide invaluable tie points for winds inferred from temperature and pressure.

#### 13.3.2.1 Indirect Methods

The shape of the zonally averaged pressure and temperature fields is linked to the mean zonal winds. For steady, inviscid, axisymmetric flow, the balance is (see, e.g., Holton 1979; Leovy 1973):

$$\frac{-\nabla P}{\rho} - \nabla V + \left(2\Omega u + \frac{u^2}{r\cos\Lambda}\right)\mathbf{i}_\perp \approx 0 \qquad (13.1)$$

where $P$ is pressure, $\rho$ is atmospheric density, $\Omega = 4.56\times10^{-6}$ s$^{-1}$ is Titan's angular rate of rotation, $u$ is the zonal velocity, $r$ is the radius (surface radius plus altitude), $\Lambda$ is latitude, and $\mathbf{i}$ is a unit vector normal to Titan's rotation axis. $V$ is the total potential (gravitational plus centrifugal) for a frame rotating at Titan's rotation rate; Titan is such a slow rotator that the gravitational component dominates:

$$-\nabla V \approx -g(r)\mathbf{i}_r, \qquad (13.2)$$

where $\mathbf{i}_r$ is a unit vector in the radial direction from Titan's center, and $g$ is the gravitational acceleration. The radial projection of (13.1) is the familiar hydrostatic equation:

$$\frac{1}{\rho}\left(\frac{\partial P}{\partial r}\right)_\Lambda \approx -g \qquad (13.3)$$

where the velocity terms involving $u$ in (13.1) have been neglected in the projection, to a good approximation. The horizontal projection along lines of constant meridian yields the gradient wind relation:

$$\left(2\Omega u + \frac{u^2}{r\cos\Lambda}\right)\sin\Lambda \approx -\frac{1}{\rho r}\left(\frac{\partial P}{\partial \Lambda}\right)_V \qquad (13.4)$$

Alternatively, the gradient wind relation can be written in terms of the gravitational potential variation along isobars:

$$\left(2\Omega u + \frac{u^2}{r\cos\Lambda}\right)\sin\Lambda \approx -\frac{1}{r}\left(\frac{\partial V}{\partial \Lambda}\right)_P \qquad (13.4)$$

The balance (13.4 or 13.4') generally holds for zonally averaged variables to a good approximation when the lateral scale is large compared to a scale height. Hence, (13.1), as well as (13.3) and (13.4), can be viewed as a hydrostatic balance law in two dimensions (in height and latitude), with the centrifugal acceleration associated with the zonal winds adding vectorially to the gravitational acceleration. A possible exception is near the equator, where the left-hand side of (13.4) becomes small because of the trigonometric term. For instance, on Earth the mean lateral convergence of momentum by eddies – not included in (13.1) or (13.4) – in the intertropical convergence zone is known to be important. Usually one does not know a priori how close to the equator the gradient wind relation fails, or even if it does: (13.4) can remain valid if $(\partial P/\partial\Lambda)_V \propto \sin\Lambda$ across the equator. In practice, errors in the measured variables preclude application of (13.4) as $\Lambda\to0$, because the errors in $u$ from the propagation of the errors on the right-hand side magnify inversely as $\sin\Lambda$ or $\sqrt{\sin\Lambda}$.

In rapidly rotating bodies, like Earth, Mars, and the outer planets, the first term on the left-hand side of (13.4, 4'), linear in $u$, dominates, and the equation reduces to geostrophic balance, in which the meridional gradient in pressure is balanced by the Coriolis force. For slow rotators, like Venus, the second term, quadratic in $u$, dominates and one has cyclostrophic balance, in which the pressure gradient is balanced by the centrifugal force associated with the zonal winds themselves. Titan is also a slow rotator, and in its middle-atmosphere the winds greatly exceed Titan's equatorial surface velocity ($\Omega a \approx 11.7$ m s$^{-1}$, where $a = 2{,}575$ km is Titan's radius); cyclostrophic balance is again dominant. Because the centrifugal force is quadratic in $u$, the direction of the zonal wind is not determined from the gradient wind relation. For the relation to hold at all, however, the pressure at constant height (or, equivalently, the potential along isobars) must decrease poleward. Hence cyclostrophic flow requires an equatorial bulge. Central flashes observed at Earth during occultations of stars by Titan have provided information on the shape of the isopycnal (i.e., constant-density) surfaces near the 0.25-mbar level (Hubbard et al. 1993; Bouchez 2003; Sicardy et al. 2006). Without too large an error, one can take these surfaces to be isobars (see Hubbard et al. 1993) and apply the gradient wind

Uncorrected Proof

equation (13.4'). Figure 13.11 (Chapter 13; Lorenz et al. 2009) illustrates the zonal winds derived from some of these occultations.

Historically Titan's cyclostrophic winds were first inferred from temperature data using the thermal wind equation (Flasar et al. 1981; Flasar and Conrath 1990). Operating on equation 13.) with the curl (∇():

$$\nabla P \times \nabla \frac{1}{\rho} + 0 + \nabla\left(2\Omega u + \frac{u^2}{r\cos\Lambda}\right) \times \mathbf{i}_{\perp} \approx 0 \qquad (13.5)$$

For axisymmetric flow, gradients around latitude circles vanish, and only the zonal component in (13.5) is nonzero. With the assumption of the perfect gas law and the neglect of spatial variations in the bulk composition (both valid except in the lower troposphere), this gives:

$$\frac{\partial}{\partial z_{\parallel}}\left(2\Omega u + \frac{u^2}{r\cos\Lambda}\right) \approx \frac{1}{P}\frac{\partial P}{\partial r}\frac{R}{r}\left(\frac{\partial T}{\partial \Lambda}\right)_P \qquad (13.6)$$

where $z_{\parallel}$ is the coordinate parallel to the planetary rotation axis. With (13.3), (13.6) reduces to:

$$\frac{\partial}{\partial z_{\parallel}}\left(2\Omega u + \frac{u^2}{r\cos\Lambda}\right) \approx -\frac{g}{T}\frac{1}{r}\left(\frac{\partial T}{\partial \Lambda}\right)_P . \qquad (13.7)$$

From (13.5), the gradient in $u$ is perpendicular both to the gradients in $P$ and in $T$. Thus the "thermal wind," resulting from the integration of Eqs. 13.5 or 13.7, lies along isotherms on isobars.

Unlike the gradient wind equation, the thermal wind equation (13.7) requires a boundary condition, a specification of $u$. Often one specifies $u$ on a lower boundary. Zonal winds derived from (13.7) are illustrated in the bottom panel of Fig. 13.2. The salient features are the strong circumpolar wind, the polar vortex, in the (northern) winter hemisphere, and the weak zonal winds in the summer hemisphere, where meridional contrasts in temperature are weaker.

For a thin atmosphere,

$$\Delta z_{\parallel} \approx \Delta z / \sin\Lambda_0, \qquad (13.8)$$

where $\Lambda_0$ is an average (constant) latitude. With this approximation eq. (13.7) reduces to the usual thermal wind equation:

$$\frac{\partial}{\partial r}\left[2\Omega u \sin\Lambda + \frac{u^2 \tan\Lambda}{r}\right] \approx -\frac{g}{T}\frac{1}{r}\left(\frac{\partial T}{\partial \Lambda}\right)_P, \qquad (13.9)$$

or in ln$P$ coordinates,

$$-\frac{\partial}{\partial \ln P}\left[2\Omega u \sin\Lambda + \frac{u^2 \tan\Lambda}{r}\right] \approx -\frac{R}{r}\left(\frac{\partial T}{\partial \Lambda}\right)_P. \qquad (13.9')$$

On Titan the relation (13.9, 9') fails at low latitudes, because the approximation (13.8) breaks down, and the integration of the thermal wind equation (13.7) to solve for the zonal winds must be along cylinders concentric with Titan's rotation axis (Flasar et al. 2005). For example, the 0.4-mbar isobar is approximately 130 km higher in altitude than the 10-mbar isobar. A cylindrical surface that intersects the equator at 10 mbar intersects the 0.4-mbar level at 17° latitude. These intersections (at northern and southern latitudes) lie on the parabola depicted in Fig. 13.2 tangent to the 10-mbar level. Outside this parabola, it is sufficient to apply a boundary condition at the 10-mbar level to integrate the thermal wind equation (13.7). However, cylinders intersecting the latitudes and pressure-levels within this parabola do not intersect the 10-mbar level. In this region, one must specify a boundary condition on the winds at higher altitudes, for example in the equatorial plane. However, the latter is a priori unknown. In Fig. 13.2 the winds within the 10-mbar parabola were interpolated along isobars. Although the winds at 10-mbar and lower are not well determined globally, this probably does not pose a critical problem in the winter northern hemisphere, as shown in Fig. 13.2. This is because the thermal wind equation implies that the winds increase markedly with altitude, and the zonal winds in the upper stratosphere are dominated by the thermal wind component above the 10-mbar level, i.e., the integral of the left hand side of (13.9, 9′). Since the $u^2$ term dominates the left-hand side of (13.7), it is not sensitive to the 10-mbar boundary condition away from the boundary. At mid and high latitudes in the southern hemisphere, the predicted thermal winds are weaker, and they are more sensitive to what is happening at the lower boundary.

Figures 13.2 and 13.11 (Chapter 13) indicate a significant seasonal variation in the stratospheric zonal winds, with the strongest velocities in the winter hemisphere. This is expected, because of the seasonal variation in temperatures (Section 13.3.1). The zonal-wind and temperature fields are coupled through the thermal wind equation, and hence changes in temperatures imply concomitant changes in the zonal winds. However, radiative processes do not transport angular momentum. It is mass motions, eddies, and waves that effect this transport and affect the nature of the seasonal variation (Sections 13.2 and 13.4).

### 13.3.2.2 Direct Methods

#### Doppler Line Shifts

One technique offering a direct determination of the wind speed and direction is to measure the differential Doppler shift of atmospheric spectral features as the field-of-view moves from east limb to west limb. Infrared heterodyne observations of Titan's ethane emission at 12 μm have been

Uncorrected Proof

performed on three separate occasions (Kostiuk et al. 2001, 2005, 2006). Although the instrument field of view covered a significant portion of Titan's disk, the measurements consistently provided evidence for eastward winds with velocities exceeding 200 m $s^{-1}$ at heights near 200 km (1 mbar), but with a relatively large uncertainty (Fig. 13.4). Luz et al. (2005, 2006) have performed similar observations over a wide range of wavelengths from 420 to 620 nm using a high performance spectrograph at the Very Large Telescope. Eastward wind with velocities of about 45–60 m $s^{-1}$ were inferred at 170–200 km altitude, the primary height range of the emission features used to determine the differential Doppler shift between east and west limb. The technique has also been extended to the millimeter wavelength range, which it is sensitive to higher altitudes, depending on the specific spectral feature measured. Moreno et al. (2005) found the atmosphere to be superrotating at a speed of $160 \pm 60$ m $s^{-1}$ (centered at 300 km altitude) and $60 \pm 20$ m $s^{-1}$ (450 km), respectively.

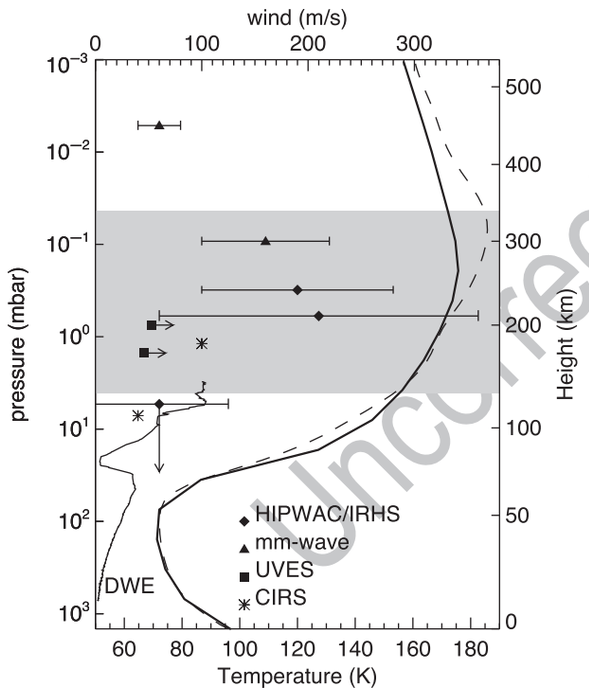


**Fig. 13.4** *Upper abscissa*. Titan zonal wind velocity determined from measurements at different heights. The DWE profile from the surface to 145 km (Bird et al. 2005) is shown for comparison. In decreasing order of height the highest two data points (*triangles*) are the mm-observations from Moreno et al. (2005). The *diamonds* show results from the heterodyne IR observations of Kostiuk et al. (2001, 2005, 2006). Luz et al. (2005, 2006) reported results from broadband UVES observations (lower bounds – *squares*). Two representative points (*asterisks*) are included from the CIRS zonal wind retrieval at 15°S (Flasar et al. 2005), adjusted to be consistent with the DWE-determined wind velocity of 55 m/s at 10 mbar. *Lower abscissa*. The temperature profiles are the *solid curve* from Yelle et al. (1997) and the *dashed curve* from Flasar et al. (2005) (reproduced from Kostiuk et al. 2006)

[AU3]

## Cloud Tracking

The measurement of winds from tracking of cloud motions has been a valuable technique on all of the giant planets and Venus. Unfortunately, Titan has not been kind to cloud trackers. Its clouds are infrequent and are typically ephemeral, lasting less than a few hours in many cases. Yet this potentially remains one of the few existing means to probe the zonal winds globally in the troposphere.

Prior to the arrival of Cassini-Huygens, disk-average ground-based observations at near infrared wavelengths in 1998 suggested the presence of reflective clouds, thought to be $CH_4$, covering less than 7% of Titan's disk and located at roughly $15 \pm 10$ km altitude (Griffith et al. 2000). Observations the following year indicated a high degree of temporal variability, with the inferred clouds dissipating in as little as 2 h. Yet they were observed over several nights. Radiative transfer modeling indicated the clouds were near 27 km altitude and covered only 0.5% of the disk, about 1% of the cover typically seen on Earth. Later observations, using adaptive optic systems that resolved Titan's disk (Brown et al. 2002; Roe et al. 2002) showed transient clouds concentrated near the south pole, which was in early summer. The authors interpreted the location and variability of the clouds as evidence of moist convection involving $CH_4$ condensation. Later observations in October 2004, shortly after Cassini's orbit insertion, showed an 18-fold increase in cloud brightness (Schaller et al. 2006a) near the south pole, with a factor-of-two change in brightness over 24 h. Earlier observations from 1996 to 1998, using speckle interferometry at the W. M. Keck Telescope (Gibbard et al. 2004), had also detected clouds near the south pole, supporting the notion that this was a long-term seasonal activity driven by the warm surface at the pole in late spring and early summer.

Later observations revealed clouds at temperate latitudes. With adaptive optics techniques at the Gemini North 8-m telescope, Roe et al. (2005) found tropospheric clouds clustered between 37° and 44°S on three of thirteen nights in 2003–2004. Unlike the nearly circular nature of the south polar clouds, these clouds were filamentary, extending eastward more than 1,000 km, about 30° in longitude, while only spanning a few degrees in latitude. These clouds were mostly clustered near 350°W, which suggested a geographical tie, associated perhaps with geysers or cryovolcanoes that could inject bursts of $CH_4$ vapor into the atmosphere. Subsequent observations by the Imaging Science Subsystem (ISS; Porco et al. 2005; Turtle et al. 2008) and the Visual and Infrared Mapping Spectrometer (VIMS; Griffith et al. 2005; Rodriguez et al. 2009) failed to corroborate the preferential location on the side of Titan facing Saturn; in fact the VIMS and ISS data indicate that the clouds in this latitude belt are nearly uniformly distributed in longitude (Rodriguez et al. 2009; Turtle et al. 2008). Other mechanisms, involving

Uncorrected Proof

meridional transports of $CH_4$, have been suggested (Griffith et al. 2005).

Observations of the motions of a few well-behaved long-lived (~1 day) clouds, led to the first cloud-tracked wind velocities from ground-based observations. Tracking a temperate latitude feature on 2–3 October 2004, Roe et al. (2005) deduced a velocity of 8 m $s^{-1}$ eastward and 3 m $s^{-1}$ northward, which seemed consistent with the expected direction and magnitude of tidal winds (Section 13.6.1). Bouchez and Brown (2005) tracked clouds over several nights near the south pole and found no significant motion, placing 3-$\sigma$ limits of 4 m $s^{-1}$ on zonal (i.e., east–west) motion, and 2 m $s^{-1}$ on meridional (north–south) motion.

The Cassini ISS and VIMS instruments both observed the south polar cloud during the first (distant) Titan flyby (T0) on 2 July 2004. Both sets of observations indicated sluggish eastward motions less than 4 m $s^{-1}$ at high southern latitudes (Porco et al. 2005; Baines et al. 2005; Brown et al. 2006). VIMS observed four cloud features, the most prominent being a 700-km wide feature centered at 88°S (Baines et al. 2005). Three smaller clouds were observed within 16° of latitude of this main feature, ranging in size from 65 to 170 km in diameter. The prominent south polar cloud was observed for 13 hours, enabling a measurement of a zonal wind speed of $0.5 \pm 3.3$ m $s^{-1}$ (Brown et al. 2006), slightly favoring an eastward motion. Two other cloud features, one at 74°S and the other at 78°S, showed slow zonal wind speeds of $0.9 \pm 3.9$ and $2.3 \pm 2.0$ m $s^{-1}$, respectively, both also consistent with eastward motions. Meridional motions were imperceptible.

The ground-based adaptive optic imagery of the south polar clouds by Schaller et al. (2006a) in October 2004, several weeks prior to the first Cassini cloud observations, also led to zonal velocity estimates. From two pairings of nights, Schaller et al. found zonal wind velocities of $2 \pm 3$ and $0 \pm 4$ m $s^{-1}$, consistent with the VIMS and ISS south polar cloud results. From VLT/NACO and CFHT/PUEO adaptive optics imagery acquired in 2002–2004, Hirtzig et al. (2006) measured an average south polar zonal wind speed of $3 \pm 2$ m $s^{-1}$. Subsequent observations between December 2004 and April 2005 showed the nearly complete disappearance of the south polar cloud (Schaller et al. 2006b), although VIMS observations have indicated periodic outbursts occurring almost every nine months from December 2004 through June 2007 (Rodriguez et al. 2009). These outbursts diminished in strength and persistence with time as the Titan equinox approached, perhaps consistent with the march of the summer season and the change in meridional transport by the global circulation.

ISS observations during the first Titan encounter (T0) showed the fastest cloud feature tracked so far: $34 \pm 13$ m $s^{-1}$ eastward at 38°S. Eastward winds were also measured for 9 of 11 other clouds. During the third Titan flyby (Tb) in December 2004, VIMS images showed a long cloud streak extending over 25° in longitude near 41°S (Baines et al. 2005). Attempts to derive reliable zonal velocities with time lapsed observations were unsuccessful. Spectral analysis of four discrete cloud features embedded within this cloud streak by Griffith et al. (2005) showed rapid changes in cloud top altitude over 35 min, with one cloud top rising 14 km in altitude during that time, from 21 to 35 km, corresponding to updraft velocities near 10 m $s^{-1}$. They also concluded that high cloud centers dissipate or descend to the ambient cloud level near 10 km within an hour, consistent with the fall velocity of millimeter-sized raindrops expected for Titan (Toon et al. 1988; Lorenz 1993). Thus, temperate latitude cloud streaks can be highly dynamic and changeable, with altitudes that can vary on short timescales. Consequently, they are not typically reliable indicators of wind velocities.

### Huygens Doppler Wind Experiment (DWE)

The Huygens probe has provided the most detailed vertical profile of Titan's zonal wind. After its heat shield was jettisoned and the first parachute deployed, the probe descended for nearly 150 min before impacting the surface near 10°S. During this descent phase, the lateral motion of the probe was close to that of the ambient winds. The DWE instrumentation, consisting of an atomic rubidium oscillator in the probe transmitter to assure adequate frequency stability of the radiated signal and a similar device in the orbiter receiver to maintain the high frequency stability, was implemented only on one of the radio links on the Cassini spacecraft, Channel A (2,040 MHz). Whereas the other link, Channel B (2,098 MHz), functioned flawlessly during the entire mission, the Channel A receiver was not properly configured during the probe relay sequence. All data on this link, including the probe telemetry and the planned DWE measurements, were lost. Fortunately, the primary DWE science objective, a vertical profile of winds on Titan, was largely recovered by ground-based tracking of the Channel A signal at large radio telescopes (Bird et al. 2005; Folkner et al. 2006).

During the DWE design phase it was recognized that Earth-based Doppler measurements could be combined with the orbiter Doppler measurements to reconstruct both the zonal and meridional components of the Huygens probe motion during descent (Folkner et al. 2004). Ideally, the horizontal projection of the ray paths from Huygens to Cassini and to the Earth should be perpendicular, but the 160° separation for the actual experiment geometry was still considered adequate for the calculation. A fundamental uncertainty in the Earth-based measurement was whether the received power from the Huygens carrier signal would be sufficient to support near real-time reduction of the data, or if a more extensive data processing effort, augmented with additional information from the telemetry sub-bands, would

Uncorrected Proof

be required, as it was in the case of the ground-based detection of the Galileo Probe signal at Jupiter (Folkner et al. 1997). Despite the considerably greater distance, the probability of detecting the Huygens signal from Titan was deemed slightly more favorable than for the case of the Galileo Probe, because of the substantially higher Huygens transmitter antenna gain toward Earth. Moreover, significant residual carrier power in the Huygens signal was expected, compared to no residual carrier for the Galileo Probe. Ground-based support was solicited in a multi-facility observation proposal submitted to the National Radio Astronomy Observatory (NRAO), specifically for observation time at the Robert C. Byrd Green Bank Telescope (GBT) in West Virginia, and at eight antennas of the Very Long Baseline Array (VLBA), and to the Australia Telescope National Facility (ATNF) for observations at the Parkes Radio Telescope and several other smaller Australian antennas.

A second Earth-based experiment designed to provide ultra-precise sky positions of the Huygens probe using the Very Long Baseline Interferometry (VLBI) technique (Pogrebenko et al. 2004; Witasse et al. 2006) was conducted in parallel with the ground-based DWE observations. The results of the VLBI experiment, which enlisted a total of 17 radio telescopes in Australia, China, Japan, and the USA, are still under review.

The topocentric sky frequencies of the Huygens Channel A carrier signal recorded at GBT and Parkes are shown in Fig. 13.5. The time resolution is typically one point each 10 seconds, for which the measurement error is of the order of 1 Hz, corresponding to an uncertainty in the line-of-sight velocity of 15 cm $s^{-1}$. The Earth-based signal detection at GBT coincides with the initial transmission from Huygens at $t_0+45^s$, where $t_0$ is the designated start of the descent. Also indicated in Fig. 13.5 are the times of impact and loss of link to Cassini. The Huygens probe was still transmitting from Titan's surface when Titan descended below the minimum elevation limit in the terrestrial sky and the signal could no longer be tracked at the Parkes antenna.

A Doppler signature for the change from the main parachute to a smaller drogue parachute may be seen in Fig. 13.5 at $t_0+15^m$. At this instant, the suddenly larger descent velocity produces an abrupt decrease in the received frequency which closely follows that predicted by simulation. An additional decrease in the observed frequency comes from the rapidly decreasing zonal wind that continues through the parachute exchange event (Fig. 13.6). Similarly, a nearly discontinuous frequency increase marks the impact on the surface at 11:38:11 SCET/UTC. The magnitude of this positive jump in frequency, 26.4 ± 0.5 Hz, reflects the abrupt change in vertical velocity from about 5 m/s to zero.

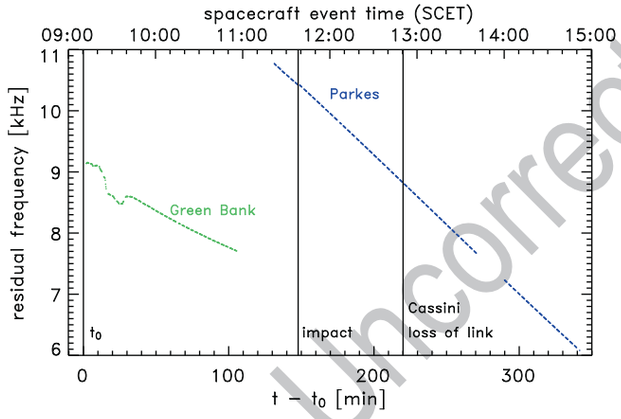


**Fig. 13.5** Topocentric sky frequencies of the Huygens Channel A carrier signal recorded at the GBT and Parkes facilities. A constant value of 2,040 MHz, the nominal transmission frequency, has been subtracted from all measurements, so that the plotted data points are equivalent to the total signal Doppler shift from transmitter to receiver. The *upper time scale* is Spacecraft Event Time; the *lower scale* is minutes past the nominal start of mission at $t_0$ = 09:10:20.76 SCET/UTC. The Earth's rotation is primarily responsible for the lower recorded frequency at GBT (*near end of track*) with respect to Parkes (*near start of track*). The *small gaps* between data segments and the larger post-landing gap correspond to intervals when the radio telescopes were pointed to celestial reference sources near Titan for calibration of the simultaneously conducted VLBI experiment. A single larger gap of 26 minutes is present in the interval between the end of the observations at GBT and the start of observations at Parkes. The times of impact at $t_0+147^m\ 50^s$ (11:38:11 SCET/UTC) and loss of link to Cassini at $t_0+220^m\ 3^s$ (12:50:24 SCET/UTC) are indicated. The Parkes tracking pass ended at $t_0+341^m\ 37^s$ (14:51:58 SCET/UTC) with the Huygens probe still transmitting from the Titan surface (after Bird et al. 2005)

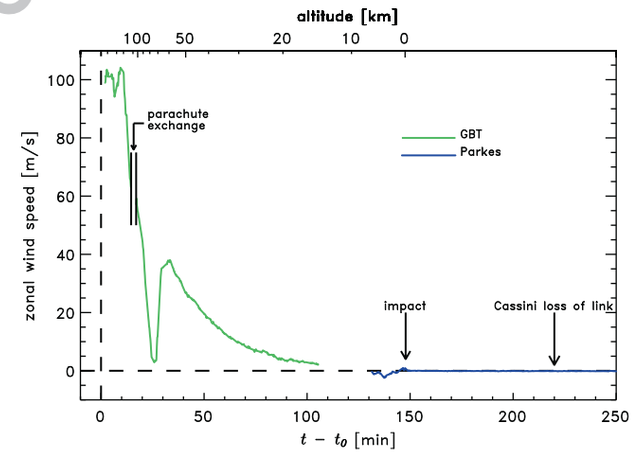


**Fig. 13.6** Zonal wind velocity during the Huygens mission. The winds above 12 km are eastward (positive zonal wind), but a significant reduction in the wind speed is observed at altitudes in the interval from 60 to beyond 100 km. The interval associated with the parachute exchange, during which the probe lags the actual wind, starts at an altitude of 111 km and lasts until 104 km. A monotonic decrease in the zonal wind speed was recorded from 60 km down to the end of the GBT track at 10:56 SCET/UTC. The Parkes observations could not begin until 11:22 SCET/UTC, thereby excluding wind determinations in the height region from roughly 12 km down to 4.5 km. By this time Huygens was in a region of weak westward winds that again turned eastward about 1 km above the surface (adaptation and update of Bird et al. 2005)

Uncorrected Proof

With precise knowledge of the geometry, the raw measurements of sky frequency yield the line-of-sight motion of the transmitter in the Titan frame of reference. The vertical motion of the Huygens probe, which slowly decreased with decreasing altitude, was measured in situ by the HASI pressure sensors (Fulchignoni et al. 2005) and the Huygens radar altimeters. The available consolidated measurements were processed iteratively by the Huygens Descent Trajectory Working Group (DTWG) to produce a series of continually improving Huygens trajectories referenced to Titan (Atkinson et al. 2007; Kazeminejad et al. 2007). The results presented here are based on the descent velocity of the final DTWG data set #4, released in May 2007. Based on knowledge of the Huygens point of atmospheric entry following separation from Cassini, and integrating the trajectory through the entry phase with the help of accelerometer measurements (Colombatti et al. 2008), the DTWG also supplied the nominal coordinates of the Huygens probe in latitude (10.33 ± 0.17°S), longitude (196.08 ± 0.25°W), and altitude (154.8 ± 8.5km) at the start of descent $t_0$.

Two key assumptions about the horizontal motion of the probe were applied to simplify the problem of determining the probe velocity during descent. The first of these is that the horizontal drift of the probe follows the horizontal wind with a negligible response time. The actual response time for the Huygens descent system is estimated to be roughly 30–40 s in the stratosphere, decreasing to 3–5 s in the lowest 10 km (Atkinson et al. 1990; Bird et al. 1997). This may be fulfilled only marginally during the early minutes of the descent and is violated briefly during the deployment of the second parachute (altitudes: 111–104 km). Barring any unanticipated parachute aerodynamics, the probe should be capable of roughly following the wind again at all altitudes below 100 km. A simple modeling analysis of the difference between the zonal wind speed and the zonal probe speed concluded that the probe was lagging the wind by up to a maximum of 7% above 40 km and that Huygens was an unreliable wind gauge only during the 2-min interval following the parachute exchange. The second assumption, that the drift in the meridional (north–south) direction is negligible, is based primarily on theoretical considerations that imply dominance of the zonal (east–west) atmospheric circulation (Flasar 1998b). The Huygens trajectory reconstructed from landmark positions determined from the DISR images below 40 km was found to have a small, but nonzero, meridional drift (Karkoschka et al. 2007). The poor projection of the north–south motion onto the line-of-sight to Earth results in a negligible effect on the observed Doppler shift and thus the zonal wind retrieval.

Small, nearly time-invariant corrections were applied for the effect of special relativity (−7.5 Hz, whereby the minus sign means a red shift), as well as the effects of general relativity associated with the Sun (18.2 Hz), Saturn (−0.7 Hz), Earth (1.4 Hz) and Titan (−0.08 Hz). A detailed discussion of these corrections may be found in Atkinson (1989). Propagation corrections to the Doppler measurements from ray refraction in the neutral and ionized intervening media (Titan, interplanetary, and Earth) have been estimated and found to be negligible. Temperature inversions, which can produce a distinct Doppler signature in the received frequency for a conventional occultation geometry with tangential ray propagation, are not effective for the case of radio propagation from Huygens to Earth because the signal propagates upward out of the atmosphere and thus parallel to any strong radial gradients. A final small correction of +10.0 Hz was applied to the absolute transmission frequency by invoking the constraint that Huygens remains stationary on Titan's surface after landing. This residual is within the error limits of the pre-launch unit-level calibration of +9.2 Hz determined for the specific DWE oscillator unit used to drive the Huygens Channel A transmitter.

The variation of the zonal wind as a function of time, derived from the data in Fig. 13.5 using an algorithm developed for the Huygens-Cassini link (Dutta-Roy and Bird 2004), but adapted for the Huygens-Earth link, is shown in Fig. 13.6. More precisely, the quantity plotted in Fig. 13.6 is the horizontal velocity of Huygens in the east direction with respect to the surface of Titan (positive value indicating the eastward direction). The time-integrated wind measurement from $t_0$ yields an estimate for the longitude of the Huygens landing site on Titan, 192.33 ± 0.31°W, which corresponds to an eastward drift of 3.75 ± 0.06° (165.8 ± 2.7 km) over the duration of the descent. This propagation error associated with the wind retrieval has been estimated and is found to be insignificant because the Doppler shift depends only weakly on the probe's position during the entire descent.

The variation of the zonal wind with altitude and pressure level is shown in Fig. 13.7 in comparison with the Titan engineering wind model and envelopes based on Voyager temperature data (Flasar et al. 1997). The measured profile is in rough agreement with the upper level wind speeds anticipated by the engineering model and generally eastward above 12 km altitude, within the region tracked from GBT. Assuming this local observation is representative of conditions at this latitude, the eastward wind speed profile provided the first in situ confirmation of the atmospheric superrotation anticipated from the Voyager temperature data. Moreover, the large ratio of the measured winds to Titan's equatorial rotation speed ($\Omega \cdot a \approx 11.7$ m s$^{-1}$, where $\Omega = 4.56 \times 10^{-6}$ radian/s, and a = 2,575 km are Titan's rotation rate and radius, respectively) validates the condition of cyclostrophic pressure balance. Over the lower altitudes (<5 km) tracked by Parkes, Fig. 13.7 indicates that the winds had shifted westward, but again turned eastward over the lowest 1 km.

The most striking departure of the measured profile from the engineering model is the region of weak wind, sandwiched above and below by regions of strong positive and negative wind shear, where the zonal wind reaches a minimum of

Uncorrected Proof

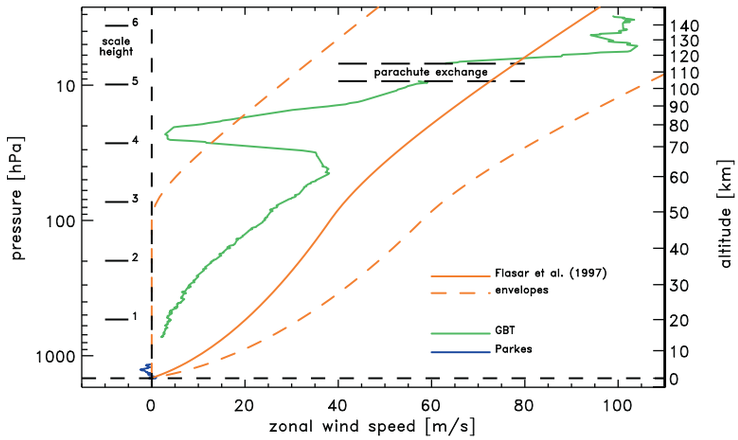


**Fig. 13.7** Titan zonal wind height profile. The zonal wind derived from GBT and Parkes observations are compared with the model and envelopes proposed by Flasar et al. (1997). With the possible exception of the region above 100 km, where the wind fluctuations are greatest, the zonal flow was found to be generally weaker than those of the model. The wind shear layer in the height range between 60 and beyond 100 km was unexpected and still lacks a generally accepted explanation (adaptation and update of Bird et al. 2005)

4 m $s^{-1}$ at about 75 km altitude. The broad minimum in zonal wind speed between 60 and 100 km, which can be seen in Fig. 13.5 as a symmetrical dip in frequency over the interval between $t_0+20$ m and $t_0+30$ m, is interpreted as a real property of Titan's atmospheric dynamics. This feature of Titan's wind profile is unlike that measured by any of the Doppler-tracked probes in the atmosphere of Venus (Counselman et al. 1980). The slow zonal wind occurs in the stratospheric region of strongest static stability, i.e., the largest vertical increase in temperature, but there is currently no generally accepted explanation of it. The thermal wind equation implies that the vertical shear in the derived zonal wind profile would be associated with strong, oppositely directed, meridional temperature gradients. Such sharp gradients might be connected with an interface region between different meridional circulation cells, but supporting observations are scarce. The slow wind layer occurs above the maximum altitude (30–40 km) for corroboration from surface feature tracking with DISR images (see below). The simultaneous VLBI tracking of Huygens had inadequate temporal resolution to verify the slow wind region (Gurvits et al., personal communication, 2009). Independent evidence in support of the strong vertical gradient in zonal wind was found in the Channel B signal amplitude measurements on the Cassini orbiter, which revealed a distinct tilt of the Huygens probe during these time intervals (Dzierma et al. 2007). The only Cassini observations that may help resolve the uncertainty in the critical height range from 60 to 100 km would be meridional temperature variations derived from either CIRS far-IR or RSS (Radio Science Subsystem) occultation data.

[AU6]

### Descent Imager/Spectral Radiometer (DISR)

The descent trajectory of the Huygens probe has been used to derive the probe ground track and extract the implied wind speed as a function of altitude (Tomasko et al. 2005). The diverse landscape near the landing site facilitated the reconstruction of the trajectory based on a sequence of images by DISR of surface landmarks. The probe moved horizontally about 2° north of east on average from the release of the first parachute to an altitude of about 50 km (Karkoschka et al. 2007). Thereafter, the motion turned slightly to about 5° south of east between 30 and 20 km altitude (Fig. 13.8, top panel). Between 15 and 6.5 km the probe moved to the east-northeast and experienced a sharp turn towards northwest (Fig. 13.8, bottom panel). Finally its motion turned counterclockwise through almost 180° at 0.7 km altitude towards the southeast or south-southeast down to the surface. No images were available during the last 200 m of the descent, so the surface wind was constrained by the direction of the parachute, which was not visible in the surface images acquired after the landing. The wind was most likely blowing towards azimuth 160° (20° east of south) with $0.3 \pm 0.1$ m $s^{-1}$. Thus the meridional wind was stronger than the zonal wind near the surface and the meridional wind changed direction at several altitudes. Throughout the descent the meridional wind speed varied between about ±1 m $s^{-1}$. The zonal winds derived from the DISR images are generally in agreement with the DWE results discussed above. In contrast to DWE, however, DISR was able to distinguish between meridional and zonal motion and could thus follow the wind direction reversals that occurred in the last minutes of the descent.

## 13.4 Meridional Circulations

Zonal-mean meridional and vertical motions are important for transporting angular momentum, energy, and constituents. Although eddy transports can be important, use of the transformed Eulerian-mean velocities incorporates many of these eddy fluxes into the mean circulation when motions are quasi-adiabatic and steady (Andrews et al. 1987). In Earth's middle atmosphere, the transformed Eulerian-mean circulation is equivalent to the Lagrangian circulation,

Uncorrected Proof

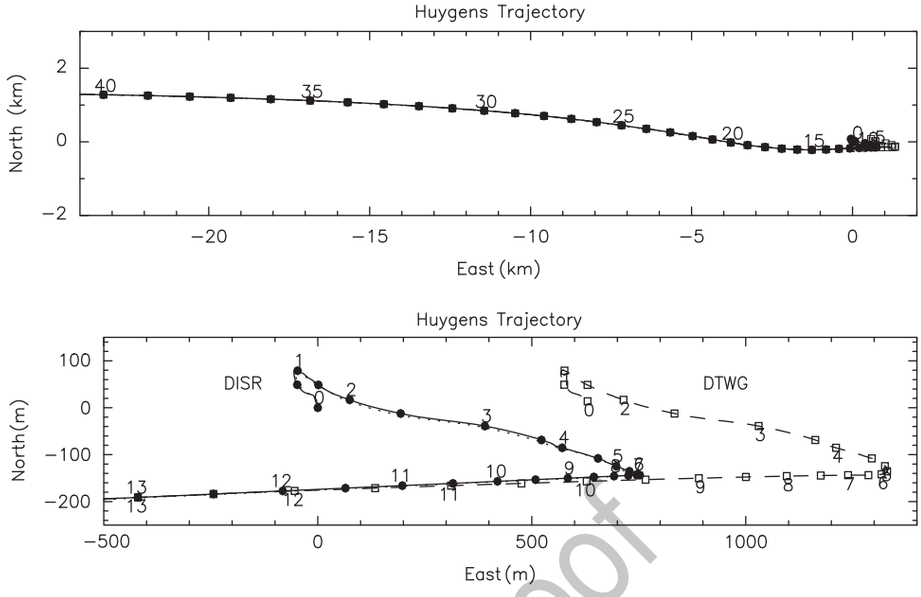


**Fig. 13.8** *Top panel.* The Huygens trajectory relative to the landing site, starting at 40 km altitude. The numbers denote altitudes in km. *Solid dots* indicate the position of Huygens every full kilometer of altitude. *Bottom panel.* The same, but starting at 13 km. Trajectories derived from DISR data alone and the DTWG determination, are both shown. The *circles* and *squares* along the curves indicate altitude at 500-m intervals. The DTWG results were based on DISR data for meridional drifts but on DWE data for zonal drifts. Below 12 km, the DTWG trajectory determination is up to ~600 m further east than that from DISR. The discrepancy likely results from the interpolation used over a gap in the DWE data between 12 and 5 km (after Karkoschka et al. 2007)

which follows the motions of conserved quantities, to a good approximation (Dunkerton 1978). There is generally no simple diagnostic relation like that between zonally averaged temperatures or pressures and mean zonal winds. One must either obtain in-situ measurements with sufficient accuracy and coverage to determine the meridional and vertical motion fields, or else one must use variables that can serve as tracers. These include, for example, gaseous constituents with lifetimes on the order of the turnover time of the meridional circulation, temperature variations along isobars, or potential vorticity (see, e.g., Flasar 1998a for more discussion of this conserved quantity) to infer the meridional circulation.

### 13.4.1 Temperatures

Flasar et al. (1981) had noted that the IRIS determination of the meridional distribution of surface temperatures, which amounted to ~3 K, was not consistent with just a radiative response to solar heating. Cassini radio occultation soundings, which cover several latitudes from 74°S to 74°N, also show a contrast of only a few kelvins in the lower troposphere. The radiative solution to the annual average solar heating would imply an equator-to-pole contrast of 15 K, far larger than observed. Flasar et al. noted that a simple Hadley circulation, annually averaged, could transport sufficient heat to reduce the meridional gradient with surprisingly small meridional velocities, ~0.04 cm $s^{-1}$.

As noted earlier, one of the most striking features of the middle atmosphere are the elevated temperatures above the north (winter) pole at the 10-μbar level. While diabatic processes involving the thick condensate hazes over the pole may be at play, adiabatic heating associated with subsidence over the pole is likely to be substantial. This is what happens in Earth's middle atmosphere (see, e.g., Andrews et al. 1987). The winter and summer seasons are marked by a cross-equatorial circulation with ascent at high summer latitudes and subsidence at high winter latitudes, within the polar vortex. The adiabatic heating over the winter pole is critical in heating the mesosphere, and indeed the mesopause over the winter pole is markedly warmer than over the summer pole because of this. Titan GCM studies are also consistent with subsidence over the winter pole (see, e.g., Hourdin et al. 2004). The lowest-order balance is between adiabatic heating and radiative relaxation:

$$w\left(\frac{\partial T}{\partial z}+\frac{g}{C_p}\right)=-\frac{T-T_{eq}}{\tau_r}, \qquad (13.10)$$

where $w$ is the transformed Eulerian-mean vertical velocity, $T$ is temperature, $C_p$ is the specific heat, $T_{eq}$ is the radiative equilibrium temperature, and $\tau_r$ is the radiative relaxation time; all quantities are zonal averages. $T$-$T_{eq}$ ~ 25 K at 10 μbar seems reasonable given the contrast between the north pole and low latitudes. At a given temperature $\tau_r$ should slowly fall off with altitude, because the decrease in mass per scale height with altitude is offset to some degree by the reduced emissivity of $CH_4$, $C_2H_2$, and $C_2H_6$, the principal infrared gaseous coolants (Flasar et al. 1981). Using $\tau_r \sim 3\times10^7$ s, appropriate to 170 K and 1 mbar, one obtains $w \sim$ -1 mm $s^{-1}$ (Achterberg et al. 2008). At 200 K, $\tau_r$ is a bit smaller and $|w|$ corresponding larger. [AU7]

Uncorrected Proof

### 13.4.2 Gas Composition

So far, the study of the meridional distribution of gases has primarily been of the organic constituents in the stratosphere. Figure 13.9 depicts the meridional variation of several organic molecules, retrieved from Cassini and Voyager thermal-infrared spectra (Teanby et al. 2005; Coustenis et al. 2007; Coustenis and Bézard 1995). All the nitriles (*HCN*, $HC_3N$, $C_2N_2$) and several hydrocarbons ($C_3H_4$, $C_4H_2$, $C_6H_6$, $C_2H_4$ in the spring) exhibit enhanced concentrations at high northern latitudes. Most of the formation of these species, following the breakup of $N_2$ and $CH_4$, occurs higher up in the atmosphere. With most organics condensing in the lower stratosphere, one expects the concentration to increase with altitude, toward the source region (Chapter 9). Limb sounding at mid-infrared wavelengths with Cassini CIRS (Vinatier et al. 2007; Teanby et al. 2007) indicates that this typically is the case. Subsidence at high northern latitudes could naturally lead to an enhanced concentration of these species at the 1–10-mbar level. Polar enhancement of the more abundant organics, e.g., $C_2H_6$ and $C_2H_2$, is less, because the vertical gradients of their concentration are smaller. Teanby et al. (2009) have noted that on average the enhancements of the various constituents scale inversely with their photochemical lifetimes. In the presence of polar subsidence, this would naturally result if the rate of increase of concentration with altitude scaled inversely with the photochemical lifetime. This seems plausible, if the mean vertical profiles of individual constituents results from a competition between vertical mixing and photochemical decay: the constituents with the shortest lifetimes will have the steepest vertical gradients in their concentration. The observed enhancements of the organics and their plausible interpretation in terms of subsidence suggests an absence of strong lateral mixing of air masses within the polar vortex with those outside by eddies or waves; this isolation also occurs on Earth at the winter pole. Analysis of limb data by Teanby et al. (2008) indicates a fairly complex structure within the winter vortex (Fig. 13.10). There seem to be areas of depletion of *HCN*, $HC_3N$, and $C_4H_2$ within the polar vortex at 300 km altitude (~0.1 mbar). What is going on has not really been worked out, but Titan's polar vortex structure seems to be as rich in structure as Earth's ozone holes.

Uncorrected Proof

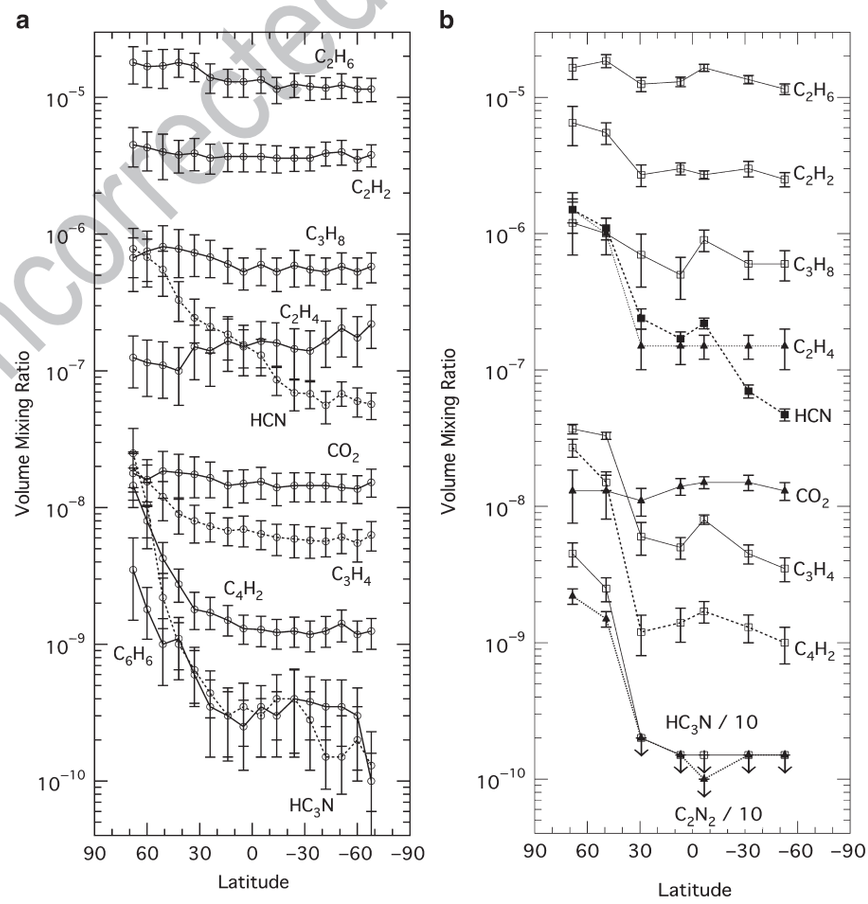


**Fig. 13.9** Meridional profiles of organic gases and $CO_2$ from nadir-viewing observations in the mid infrared in northern spring (Coustenis and Bézard 1995) and in northern winter (Coustenis et al. 2007). The spectral emission features used to retrieve the profiles typically have maxima in their contribution functions at a level of several mbar, with a spread of several scale heights. The values of $C_2H_6$ shown in the figure should be multiplied by 0.7, owing to a recently improved determination of its spectroscopic constants (Vander Auwera et al. 2008). (**a**) Cassini CIRS (2004–2005): northern winter and (**b**) Voyager IRIS (1980): early northern spring. Note that theabundances of $HC_3N$ and $C_2N_2$ in (**b**) have been offset by a factor of 10 for clarity (after Flasar and Achterberg 2009)

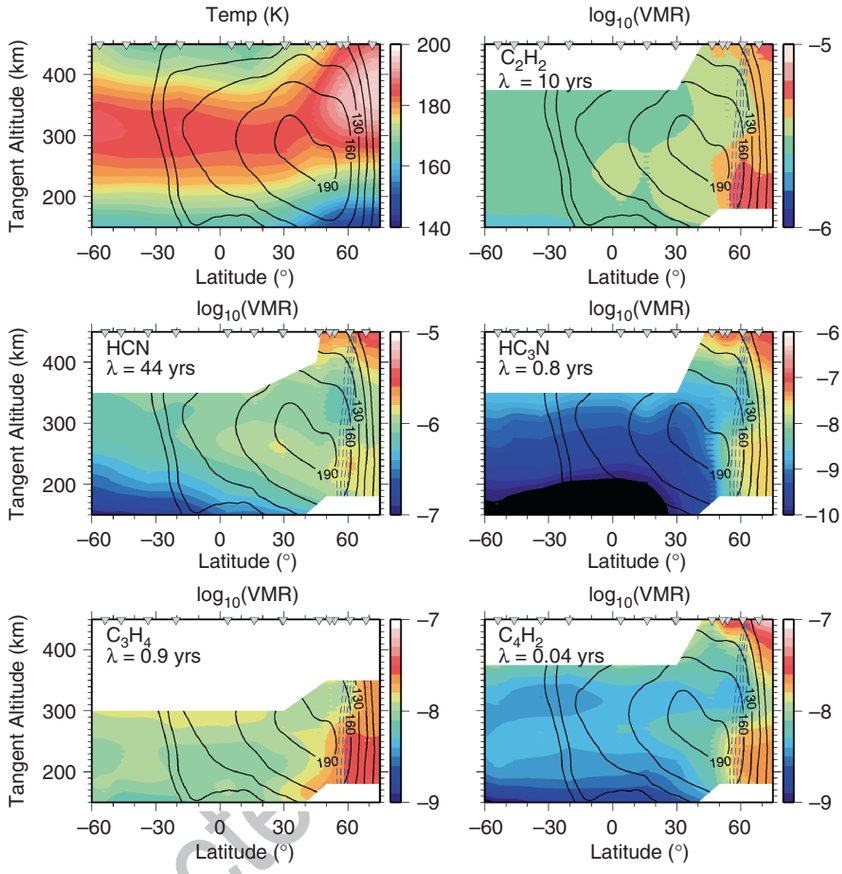


**Fig. 13.10** Cross sections of temperature (*upper left panel*) and composition from CIRS mid-infrared limb sounding. Composition is given as a volume mixing ratio and the position of the observed limb profiles are denoted by the *inverted triangles* at the top of each plot. *Contours* indicate the vortex zonal wind speeds (in m $s^{-1}$ ) derived by Achterberg et al. (2008a) and *blue dashed lines* show the region with the steepest horizontal potential vorticity gradient, which indicates a dynamical mixing barrier. Altitudes with low signal-to-noise or where the atmosphere becomes opaque are not plotted. Note that southern latitudes are toward the left of each panel. VMR denotes the volume mixing ratio and λ is the photochemical lifetime at 300 km (after Teanby et al. 2008)

### 13.4.3 Aerosols and Condensates

That Titan has an enhanced haze layer over its winter pole, suggestive of organic ices, has been known since the Voyagers flew past in 1980–1981. The haze signature is evident in images of Titan throughout the ultraviolet, visible and near infrared, because the haze structure and sometimes also particle single scattering albedo differ significantly from those at lower latitudes. Some tentative identifications of organic ices have been made, but others remain unknown. [AU10] Recent VIMS observations (Griffith et al. 2006) have detected a bright feature extending poleward of ~50° N, which is consistent with a dense $C_2H_6$ cloud located between 30 and 50 km altitude. Voyager IRIS and Cassini CIRS spectra both exhibit broad spectral features that are suggestive of condensates (Samuelson et al. 1997, 2007; Khanna 2005; Coustenis et al. 1999), but only at high latitudes in the hemisphere that is in winter or early spring. A particularly striking broad feature centered at 221 $cm^{-1}$, seen both IRIS and CIRS spectra, has yet to be identified. It may be a blend of organic ices. However, it is constricted in latitude, evident poleward of 55°N, but abruptly disappearing at 50°N and equatorward (Flasar and Achterberg 2008). This distribution does not directly provide information on meridional velocities, but it is consistent with a mixing barrier between low- and high-latitude air masses, much as occurs on Earth. It is tempting to wonder whether heterogeneous chemistry occurs on these condensates, much as it does in the terrestrial polar stratospheric clouds, but as yet there is no evidence of this.

In addition to the structure over the winter pole, there is also a more subtle hemispheric albedo asymmetry that is most noticeable in the strong methane absorption bands at 890 nm and at longer wavelengths. The boundary is displaced by about 15° from the equator. Analysis of Hubble Space Telescope (HST) images (Lorenz et al. 1997) led to the idea that hemispheric contrasts are produced by aerosol microphysical variations in the region above 70 km altitude and mostly below 120 km altitude driven by seasonal variations in aerosol transport by winds, in agreement with (but more specific than) the view that Sromovsky et al. (1981) put forth. Karkoschka and Lorenz (1997) derived haze aerosol radii near 0.3 μm in the northern latitudes versus 0.1 μm in the south from 1995 HST images of Titan's shadow on Saturn. They assign these particle radii to different layers, the 'detached haze' layer at northern latitudes and the main haze layer at latitudes south of 50ºS. Pentaedo et al. (2008) found that hemispheric variations in surface albedo and in haze optical depth and single scattering albedo at altitudes

Uncorrected

higher than 80 km account for hemispheric differences observed in Cassini VIMS spectra.

Roman et al. (2009) analyzed albedo patterns in 20 images obtained by the Cassini ISS instrument with the 890-nm methane filter (sensitive to haze above about 80 km altitude). These images reveal a haze hemispheric asymmetry with offset 3.8° ± 0.9° in latitude directed 79° ± 24° to the west of the sub-solar longitude. This result is very close to that derived by Achterberg et al. (2008b) from thermal data (Section 13.3.1) and indicates a zonal wind pattern that transports haze in accord with expectations from the thermal wind equation.

Hemispheric asymmetry in haze properties must be related to the meridional circulation but the details have not been worked out. The contrast boundary near the equator would suggest that two cells are operative in addition to a winter polar vortex. A fully coupled chemical, dynamical and haze microphysical model is needed to relate the haze observations to other processes. Some progress has been made in this area, using two-dimensional GCMs with parameterized eddy fluxes (see, e.g., Hourdin et al. 2004; Crespin et al. 2008).

### 13.4.4 In-situ Measurements

Section 13.3.2.2 has already discussed the use of DISR images to infer meridional motion during the Huygens probe descent (Fig. 13.8). Below 40 km, the meridional wind speed varied between about ±1 m s$^{-1}$. Near the surface the meridional wind was stronger than the zonal wind and both changed direction at several altitudes.

While the horizontal components of the atmospheric flow could be determined by the Doppler Wind Experiment and probe ground tracking, the smaller vertical component could not be separated from the trajectory by such means. However, the vertical wind along the descent trajectory of Huygens was determined from HASI accelerometer measurements combined with accurate knowledge of the atmospheric pressure and temperature profile during the Huygens descent. Mäkinen et al. (2006) solved the equation of motion of the descending probe using these data to determine the vertical wind speed. The measured vertical profile of vertical wind can be broadly subdivided into the stratosphere and troposphere (Fig. 13.11). In the entire troposphere the prevailing motion is upward, with a mean vertical speed of 5 cm s$^{-1}$ and several wiggles are superposed. In contrast to the troposphere, the vertical flow in the stratosphere was found to be mostly downward, with maxima at 70 and 110 km altitude (up to 0.6 m s$^{-1}$). The vertical flow around 90 km was upward (15 cm s$^{-1}$). When compared with the horizontal wind profile (Bird et al. 2005; Folkner et al. 2006), the averaged zonal and vertical profiles loosely correlate with each other, the

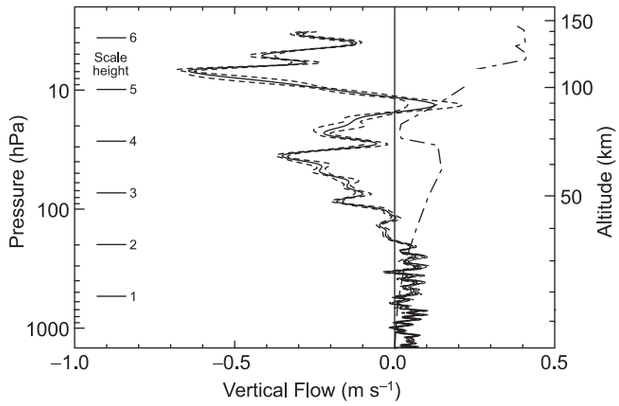


**Fig. 13.11** *Solid curve*: vertical atmospheric velocity along the descent trajectory of the Huygens probe. *Dashed curves*: the error envelope. *Dot-dashed curve*: Zonal wind derived from the Huygens DWE, scaled down by a factor of 1/250 (after Mäkinen et al. 2006)

strength of the vertical wind being about 1% of that in the zonal direction.

The large vertical velocities obtained from the probe data cannot be indicative of the zonal mean flow. To see this, consider the situation near 110 km (7 mbar), where Fig. 13.11 indicates a subsidence ~0.5 m s$^{-1}$, and the implications from the heat equation balance (13.10). At this altitude $\left(\frac{\partial T}{\partial z}+\frac{g}{C_p}\right) \approx 1.6$ K km$^{-1}$. Flasar et al. (1981) estimated the radiative relaxation times (at 10 mbar) ~$3\times10^7$ s–$1\times10^8$ s, where the larger value corresponds to just gaseous cooling by $C_2H_2$, $C_2H_6$, and $CH_4$ and the smaller value includes cooling by aerosols in a simple model. More recent estimates of radiative cooling by the Huygens DISR experiment (see Chapter 9, Fig. 9.5) yield a larger value: $\tau_r \sim 3\times10^8$ s at 110 km. One can solve (13.10) for the departure of the atmospheric temperature from the radiative equilibrium solution, which scales linearly with $\tau_r$. Using the smallest value, $3\times10^7$ s, leads to the estimate $T\text{-}T_{eq} \sim 24{,}000$ K, which is so large it can be ruled out by existing data.

Could the retrieved vertical velocities be indicative of wave motions? For the simplest case of waves propagating vertically and zonally in a mean zonal wind $\overline{u}$, the heat balance in adiabatic flow becomes:

$$w\left(\frac{\partial T}{\partial z}+\frac{g}{C_p}\right) \approx -\frac{\partial T}{\partial t}-\overline{u}\frac{\partial T}{\partial x}=i\left(\omega-\overline{u}k\right)\Delta T=\hat{\omega}\Delta T \quad (13.11)$$

where $x$ is the zonal (east–west) coordinate, $k$ is the zonal wavenumber, and $T=\Delta T exp i(kx-\omega t)$ is assumed. The quantity $\hat{\omega}$ is the (doppler-shifted) frequency of the wave relative to the background flow. For gravitational tides, which have been extensively studied (Section 13.6.1), $\hat{\omega} \sim \Omega \approx 4.6\times10^{-6}$ s$^{-1}$, the diurnal frequency (Tokano and Neubauer 2002;

Uncorrected Proof

Strobel 2006; Walterscheid and Schubert 2006), which implies a diurnal amplitude $\Delta T \sim 175$ K; this is still much too large compared to observations. Internal gravity waves may be a possibility, because they have higher frequencies. For these, $\hat{\omega}$ is bounded (see, e.g., Andrews et al. 1987) by the Brunt-Väisälä frequency,

$$\sqrt{\frac{g}{T}\left(\frac{\partial T}{\partial z}+\frac{g}{C_p}\right)} \approx 0.004\,\mathrm{s}^{-1},$$

and the Coriolis frequency, $2\Omega \sin\Lambda \sim 10^{-5}$ s$^{-1}$. From (13.11) $\Delta T \propto 1/\hat{\omega}$, implying smaller temperature amplitudes, so this suggestion merits further study.

## 13.5 Surface-Atmosphere Coupling

### 13.5.1 Structure of PBL

The planetary boundary layer (PBL) is the lowermost portion of the atmosphere that is affected by surface friction. The PBL lies below the "free atmosphere," discussed earlier (Section 13.3.2.1), where the gradient-wind balance typically holds for zonally averaged variables, at least away from the equator. The structure of the PBL controls the surface-atmosphere exchange of energy, momentum and matter, thus affecting meteorology and exogeneous geology. The first information on Titan's PBL came from the radio occultation experiment of Voyager 1, with a published altitude resolution of 0.5 km near the surface (Lindal et al. 1983). The retrieved temperature profiles near the equator, for an assumed $N_2$ atmosphere, showed a lapse rate of 1.38 K km$^{-1}$ below about 3.5 km, close to the dry adiabatic lapse rate, and an abrupt drop to 0.9 K km$^{-1}$ above this level. The lapse rate below 1 km in the evening profile (ingress) was slightly larger than the morning profile (egress). Hence the surface may have had a slight cooling effect on the atmosphere during the nighttime.

The first in situ investigation of the PBL structure was carried out by the Huygens probe, which landed near the equator in the morning hours (Tokano et al. 2006). Simultaneous vertical sounding of temperature and pressure with an altitude resolution of about 10 m near the surface was used to calculate the vertical profile of potential temperature, which is a measure of the static stability (the lapse rate in temperature less the dry adiabatic lapse rate) and a major classification criterion of a PBL. The potential temperature slightly decreased with altitude in the lowest 10 m, virtually stayed constant between 10 and 300 m and increased almost monotonically with altitude above 300 m. In other words, the lapse rate was superadiabatic immediately above the surface, adiabatic in the main part of the PBL and subadiabatic outside the PBL. Thus the 300-m PBL determined by Huygens was shallower than the 3.5-km thick layer indicated by the Voyager radio occultation data.

The observed vertical profile is indicative of a convective PBL in that the static stability is slightly unstable throughout the PBL. Based on the PBL depth the mean eddy diffusivity in the PBL is estimated as $7.4 \times 10^{-3}$ m$^2$ s$^{-1}$, which is several orders of magnitude smaller than that in a terrestrial convective PBL. Furthermore the slope of the near-surface potential temperature gradient points to an instantaneous upward sensible (convective) heat flux of 0.02 W m$^{-2}$ at the time and place of the probe landing. This indicates that the ground temperature was slightly higher than the air temperature immediately above the surface.

The small eddy diffusivity suggests very weak turbulence in Titan's PBL. This is also confirmed by in situ tilt measurements by the Huygens Surface Science Package (Lorenz et al. 2007), which experienced a calm descent in the lowest few kilometers. The presence of a weakly convective PBL without significant convective or stable stratification on Titan can be understood as an immediate consequence of the weak sunlight at Titan's surface (Tokano et al. 2006). The resulting small diurnal variation in the ground surface temperature can create only a minor temperature difference between the surface and atmosphere at any time, so the surface heat flux responsible for the heating or cooling of the atmosphere from below is always quite limited.

The wind speed in the PBL can be estimated as less than 0.3 m s$^{-1}$ (Karkoschka et al. 2007) and most likely much less than this (Folkner et al. 2006; Lorenz 2006). The vertical variation of the wind direction above the surface (Section 13.3.2.2, Fig. 13.8) does not exhibit the terrestrial Ekman–spiral behavior that typifies the frictionally controlled transition between the free-atmosphere aloft in gradient-wind balance, and the surface, where the winds vanish (see, e.g., Holton 1979). GCM simulations (Tokano 2007) indicate that the sharp reversals of the wind direction observed at two altitudes between 7 km and the surface (Section 13.3.4; Karkoschka et al. 2007) mark the boundary [AU11] of the northward and southward branch of the Hadley circulation and the altitude of the reversal of the meridional temperature gradient (Fig 13.12). The GCM studies indicate that the force balance in Titan's PBL is one in which the instantaneous pressure gradient force is balanced by Saturn's gravitational tidal force rather than by eddy diffusion, as on Earth. Hence the forces governing the PBL on Titan appear to be substantially different from those controlling a typical terrestrial PBL.

The PBL structure at other latitudes cannot be obtained from remote sensing data with this precision, but a larger seasonal variation can be expected than at the equator.

Uncorrected Proof

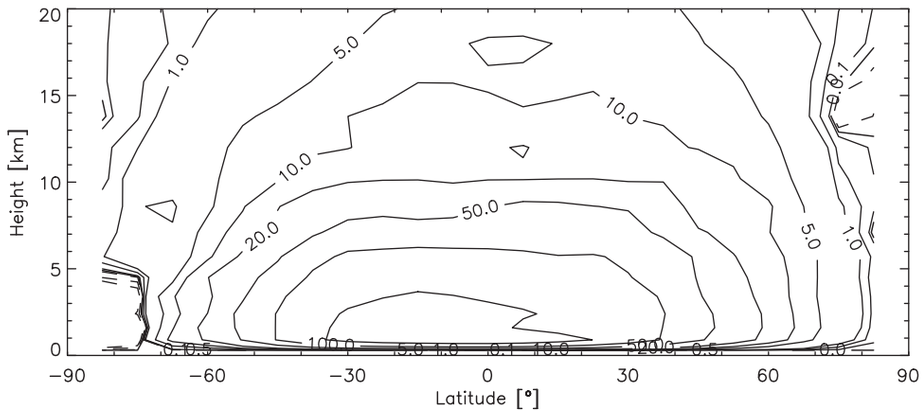


**Fig. 13.12** Mass stream function (in $10^8$ kg $s^{-1}$) of the Hadley circulation in the Huygens season from a GCM simulation (Tokano 2007). The flow is clockwise/anti-clockwise along solid/dashed streamlines. Note that southern latitudes are toward the left

### 13.5.2 Energy Exchange

The energy exchange at the surface importantly affects the general circulation of the atmosphere, because the diabatic heating that drives the atmospheric circulation experiences a sharp transition at the atmosphere-surface boundary. Prior to the Huygens mission the surface energy balance could only be estimated based on theoretical models. McKay et al. (1991) evaluated the various energy terms at the surface using a radiative-convective model that fits the observed vertical temperature profile. Approximately 10% of the sunlight arriving at the top of Titan's atmosphere reaches the surface, of which about a fifth is reflected back to space. To maintain thermal equilibrium at the surface, warming from absorbed solar radiation must be balanced by cooling from a net loss of thermal radiation and from convection. Most of the thermal infrared radiation emitted from the surface is radiated back to the surface by the greenhouse effect (collision-induced absorption) of the major tropospheric gases (nitrogen, methane and hydrogen), raising the surface temperature by 12 K over the effective surface temperature.

Haze and methane absorption coefficients and radiative fluxes measured during the Huygens probe descent through the atmosphere were used to calculate the net radiative fluxes (Tomasko et al. 2008). The net solar flux reaching Titan's surface nicely matches the estimate based on radiative-convective models (McKay et al. 1991), and there was a slight excess in the net heating as can be expected for low latitudes.

In addition to radiation, a small convective heat flux at the surface, corresponding to 1% of the incident solar flux at the top of the atmosphere, is required to explain the observed temperature profile (McKay et al. 1991; Lorenz and McKay 2003). This convective heat flux agrees with the inferred sensible heat flux of 0.02 W $m^{-2}$ at the Huygens site (Tokano et al. 2006) within the estimated error. While this small heat flux usually causes merely a shallow weakly unstable PBL, it may occasionally manifest itself as convective plumes. Lorenz et al. (2005) considered the heat engine theory for convection, which assumes that steady-state convection is just strong enough that the work available from the heat engine balances the viscous dissipation opposing the convective motions. They concluded that convective events on Titan may be rare and cover only a very small area but they may be quite violent.

Given that most of Titan's surface is not covered by an ocean, particularly not at low latitudes, latent heat exchange at the surface may not be relevant for the energy balance in most regions. Numerous extended seas and lakes, however, are present near the north pole (Stofan et al. 2007) and possible seasonal evaporation of lakes (Mitri et al. 2007; Lunine and Atreya 2008) might affect the surface energy balance. This may also be the case if there is additional liquid methane in the surface material in contact with the atmosphere (Mitchell 2008).

In an early study of moist convection using a simple buoyancy parcel model with entrainment, Awal and Lunine (1994) concluded that even if moist convection contributed to the globally averaged surface energy balance the fraction of the surface area covered by updrafts would be $10^{-5}$–$10^{-7}$, much smaller than the fraction $10^{-3}$ that characterizes the terrestrial intertropical convergence zone. Numerical models of moist convection (Hueso and Sánchez-Lavega 2006; Barth and Rafkin 2007) predict that convective clouds similar in shape to those observed near the south pole can develop if a warm bubble triggering moist convection is imposed near the surface and the methane humidity is higher than at the Huygens entry site. These clouds are characterized by a narrow updraft region in the core of the cloud with vertical wind speeds of typically 10–20 m $s^{-1}$ surrounded by large downdraft regions with weaker vertical wind. The Cassini VIMS observed the evolution of clouds residing between 41°S and 61°S (Griffith et al. 2005). The sequence of cloud images indicated vigorous updrafts of up to 10 m $s^{-1}$ in these clouds. Models also predict substantial horizontal winds converging

Uncorrected Proof

to or diverging from the clouds. However, since there are no reliable data of methane abundance in the polar region and several other hypotheses for the formation of south polar clouds have been proposed, it is still uncertain how moist convection on Titan is triggered. Particularly, the overall small horizontal and temporal variation in the near-surface temperature might not be conducive to the development of required warm bubbles.

### 13.5.3 Momentum Exchange

An important side effect of atmospheric circulation is the torque exerted by the wind on the surface, by which angular momentum is exchanged between the atmosphere and surface. Since the total angular momentum in the solid body-atmosphere system is conserved except for negligible change from external torques, angular momentum exchange at the surface gives rise to a temporal change in the planetary spin rate. On Earth the alternating sequence of net acceleration and deceleration of the spin rate by varying surface winds causes an annual variation of the length-of-day (LOD) of roughly 1 ms.

Tokano and Neubauer (2005) pointed out that similar effects should be expected on Titan, because it is covered by a dense atmosphere and the tropospheric winds they predict are variable on seasonal timescales. They calculated the seasonal change in the atmospheric angular momentum using the global zonal wind field predicted by a general circulation model (GCM) as is also common practice in Earth's geodesy. The predicted seasonally exchanged angular momentum amounts to ~$3\times10^{25}$ kg m$^2$ s$^{-1}$, roughly comparable to that on Earth, and undergoes a semiannual cycle. This temporal change arises because at any instance the net angular momentum flux from the surface to the atmosphere in some regions and vice versa in other regions cannot be immediately balanced. The seasonal reversal of the zonal wind in the lower troposphere in response to the reversal of the meridional temperature gradient is the major driver for the angular momentum exchange.

The momentum exchange at the surface itself depends on the PBL structure. Angular momentum has to pass the planetary boundary layer, in which the vertical transport of momentum is characterized by eddy viscosity. The characteristic diffusive time scale for momentum to cross the PBL can be given as

$$t_{PBL} = \frac{H_{PBL}^{\ 2}}{K_{PBL}} \tag{13.12}$$

where $H_{PBL}$ is the depth of the PBL and $K_{PBL}$ is the eddy viscosity in the PBL. With $H_{PBL}$ 300 m and $K_{PBL}$ =$7.4\times10^{-3}$ m$^2$ s$^{-1}$ inferred at the landing site of the Huygens probe (Tokano et al. 2006), the diffusive time scale amounts to about $5\times10^6$ s (4 Titan days), much shorter than a Titan season. Although the eddy viscosity at other latitudes is unknown, this estimate indicates that the diffusive time scale in the PBL is short enough to allow seasonal exchange of angular momentum as predicted by Tokano and Neubauer (2005).

The major difference from Earth with respect to the seasonal angular momentum exchange is the large rotational response of Titan's solid body. The small radius and slow spin rate reduces the moment of inertia of Titan by several orders of magnitude and a seasonal LOD variation of up to 400 s is predicted, i.e., it would be 5 orders of magnitude larger than on Earth, but it also crucially depends on the yet unknown interior structure.

Repeated observations of surface landmarks by the Cassini RADAR indicate that Titan indeed rotated 0.36° per year faster than synchronous during 2004–2007 (Lorenz et al. 2008). Although the surface moment of inertia is yet unknown, the observations constrain the amount of angular momentum exchanged during this period to $2\times10^{24}$–$7\times10^{25}$ kg m$^2$ s$^{-1}$, thus consistent with the prediction by Tokano and Neubauer (2005). This large amount is only possible with a substantial seasonal variation in the zonal wind field, particularly of wind direction, in the lower troposphere. Conversely, the seasonal change in LOD has no influence on the atmospheric circulation.

The observations by the Cassini RADAR, however, indicate that the spin rate seems to be accelerating (Lorenz et al. 2008), while the model of Tokano and Neubauer (2005) predicted a decelerating spin rate during this period. Although an explanation for this discrepancy has not yet been given, such information may be useful in constraining the momentum exchange and may hold clues to general circulation of the troposphere that is otherwise difficult to constrain on Titan.

The global surface wind pattern relevant for the surface momentum exchange can be constrained by aeolian features, which represent a geological fingerprint of the surface winds. Dunes cover a large fraction of low latitudes of Titan and are mainly oriented in the east–west direction (Lorenz et al. 2006; Radebaugh et al. 2008). Morphologically, the dunes resemble longitudinal dunes in terrestrial deserts. Their observed properties on Titan then imply that the low-latitude surface winds are generally westerly (i.e., eastward). The Huygens DISR images and DWE tracking also indicated westerlies just above the surface (Section 13.3.2.2) at low latitudes (10°S). This is puzzling, since the equatorial surface is the least likely place for westerlies to form and not a single Titan GCM predicts persistent equatorial surface westerlies. For instance, the lower return leg of the Hadley cell on Earth tends to produce westward (i.e., subrotating) winds at low latitudes – the trade winds – because of the

Uncorrected Proof

combination of surface friction and angular momentum conservation (Section 13.7). The mechanism for the maintenance of eastward low-latitude winds on Titan is not yet understood, but it would have a significant effect on the global angular momentum cycle as well as momentum exchange at the surface. The surface wind cannot be everywhere and always westerly since the surface would continuously decrease the atmospheric angular momentum and accelerate Titan's rotation, so the question becomes, where are the trade winds?

## 13.6 Waves and Their Effect on the General Circulation

Waves are of dynamical interest because of their ability to transport angular momentum and energy over large distances and because they can serve as a probe of the background flow, i.e., structure of winds and stability. Hinson and Tyler (1983) analyzed intensity scintillations in the Voyager radio occultations and in the stratosphere found them to be consistent with small-scale internal gravity waves. Analysis of waves in the Cassini radio occultations is as yet incomplete. The possibility that internal gravity waves might explain the vertical velocities derived from the Huygens descent data has been noted (Section 13.4.4). No evidence has yet been seen of thermal waves in the mapping (primarily of the middle atmosphere) by Cassini CIRS. For instance, the discovery of the pole tilt in the stratosphere at 1 mbar (Section 13.2.1) resulted from a search for zonal structure in the temperature field (Achterberg et al. 2008b). The dominant mode was the wavenumber-1 feature that corresponded to the pole tilt. When this is removed from the temperature field, the residual variance is comparable to the instrument noise. Analysis of the residuals is not complete, however, and further work is needed.

The remainder of this section discusses gravitational tides on Titan, which have been extensively studied.

### *13.6.1 Gravitational Tides*

Atmospheric tides can be subdivided into thermal tides caused by the apparent motion of the Sun radiatively forcing the atmosphere and gravitational tides raised by an adjacent moon or planet. In the atmospheres of Earth, Mars and Venus only thermal tides are of importance. For instance, the lunar atmospheric tide on Earth causes a surface pressure variation of less than 0.1 mbar, much smaller than the pressure variation caused by weather systems (Chapman and Lindzen 1970). The gravitational tide generally becomes more relevant on outer planets because they are massive and receive little sunlight.

The gravitational tide on Titan is caused by the difference between the centrifugal force of Titan and Saturn's gravitational force, which varies spatially across the body of Titan. The tidal flow is a result of the time-dependent part of the tidal acceleration associated with Titan's orbital eccentricity (0.0292). The combination of radial and librational tidal components gives rise to a semidiurnal tide that circles Titan eastward with half of Titan's angular velocity, while the tidal potential at a given location oscillates with a period of 1 Titan day (Fig. 13.13). This tide acts equally on the entire atmosphere as well as Titan's interior. There is also a stationary and a westward propagating tidal component with wavenumber 2, but the latter one is seven times weaker than the eastward propagating or stationary component (Walterscheid and Schubert 2006). In principle, atmospheric tides can perturb Titan's external gravitational potential, both from the displacement of the atmosphere itself and also from the redistribution of mass within Titan induced by the variable atmospheric loading. In practice both effects are likely negligible (Karatekin and Van Hoolst 2006).

The influence of Saturn's gravitational tide on Titan's atmospheric dynamics was investigated by Tokano and Neubauer (2002) in the framework of a general circulation model. The most obvious effect is the surface pressure variation associated with displacements of large atmospheric masses. At a given location the surface pressure varies with a period of a Titan day by up to 1.5 mbar, thus approximately 0.1%, but there is also an eastward migration of the whole surface pressure pattern with a constant phase speed as with the tidal acceleration. This tidally caused pressure variation is superposed on the meridional surface pressure gradient caused by differential heating (Hadley circulation), which is comparable in magnitude but has almost no diurnal variation.

Another important effect is the tidal wind, which significantly distorts the general circulation. In the lower troposphere where the zonal wind is weak the tidal force is one major force that balances the pressure gradient force (Tokano 2007). Near the surface the tidal wind is characterized by rotating winds (whirls), at least at high latitudes. Near the equator the tidal wind is not very apparent since the cross-equatorial flow is relatively strong (Tokano 2008a).

In most parts of the troposphere the typical speed of the tidal wind is 2 m $s^{-1}$, and is superposed on the mainly zonally oriented background wind. It causes a planetary wave of wavenumber 2 that travels eastward with the phase speed of the tide. Since these waves are linear and stable they do not amplify or decay.

Verification of the gravitational atmospheric tide on Titan is a difficult task and there is as yet no firm proof thereof. For instance, as noted above, there is no unambiguous

Uncorrected Proof

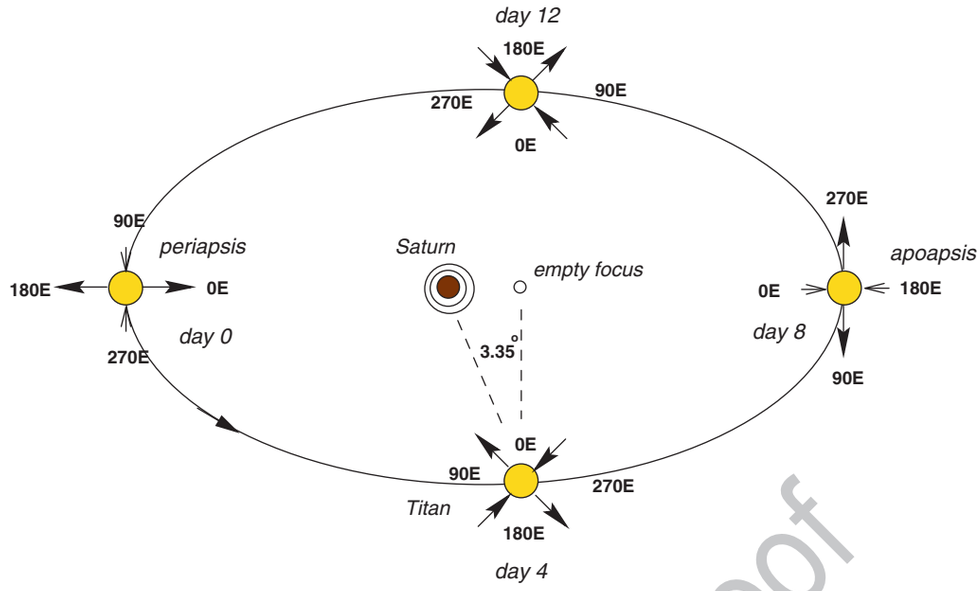


**Fig. 13.13** Titan's orbital motion around Saturn and the gravitational tide. The time-dependent component of the tidal-raising force is illustrated by *arrows* for different orbital phases. The combination of radial and librational tide causes the direction of tidal forcing to move eastward on Titan. At periapsis the radial tide peaks at the sub-Saturnian and anti-Saturnian points and the librational tide disappears. The ellipticity of Titan's orbit is exaggerated in the figure. The time-independent part of the tide is not shown because it does not contribute to tidal wind (after Tokano and Neubauer 2002)

evidence in the retrieved temperatures. It is uncertain whether the meridional drift of the Huygens probe can be ascribed to tides (Tokano 2007). Point measurements of pressure and wind as performed by Huygens are generally not sufficient since spatial and temporal variations rather than particular wind speeds or directions characterize the atmospheric tides.

In addition to in situ forcing, gravitational tides also propagate vertically and affect the dynamics of the upper atmosphere (Strobel 2006). Because of the $\rho^{-1/2}$ growth in amplitude of the tidal fields with altitude, the tidal waves attain non-linear saturation amplitudes, because the local lapse rate in temperature becomes superadiabatic. The wind and temperature above 300 km undergo large oscillations with a vertical wavelength of typically 100–150 km above 500 km altitude. The amplitude of the tide is also strongly dependent on the background zonal wind speed. The oscillating vertical temperature profile in the upper atmosphere measured by Huygens (Fulchignoni et al. 2005) resembles the predicted temperature profile in the presence of tides (Strobel 2006). These tides carry significant amounts of energy and momentum vertically and are expected to provide additional heating in the range of 500–900 km by deposition of tidal energy.

Both Strobel (2006) and Walterscheid and Schubert (2006) have suggested that gravitational tides can account for the detached haze layers that have been observed above 500 km in Voyager and Cassini images (Smith et al. 1981; Porco et al. 2005), but they emphasized different mechanisms. Strobel suggested that the temperature oscillations ~ several kelvin associated with vertically propagating tides could lead to hydrocarbon condensation at discrete levels. Although there is no evidence of these amplitudes in the CIRS nadir mapping at 200 km, temperatures retrieved from stellar occultation at altitudes 300–600 km (Sicardy et al. 1999) did show fluctuations ~4–20 K in this range. Walterscheid and Schubert (2006) emphasized that vertical transport of preexisting aerosol particles by the tide could result in discrete layers. According to their calculation the more weakly forced westward propagating tide played the major role.

## 13.7 Titan's General Circulation

### 13.7.1 Thermally Direct and Indirect Circulations

One major component of general circulation in the lower planetary atmosphere is the thermally direct circulation (warm air rises, cold air sinks) in the meridional-vertical plane, the Hadley circulation, which results from a conversion of the available potential energy supplied by the solar heating into kinetic energy. Analytical models of the general circulation (e.g. Held and Hou 1980; Schneider 2006) show that on slowly rotating planets the Hadley circulation extends to higher latitudes than on Earth, since the smaller Coriolis

Uncorrected Proof

parameter makes it more difficult for meridional temperature gradients to exceed the threshold for baroclinic instability. On Earth, this instability gives rise to the pattern of cyclones and anticyclones, which provide much of the eddy heat and momentum transports at mid latitudes. Although the temperature profile and atmospheric composition of Titan were unknown prior to the Voyager mission, Leovy and Pollack (1973) estimated that Titan's Hadley circulation would readily extend from the equator to the poles and the equator-to-pole temperature contrast would be tiny. This implies that a thermally indirect circulation, like the eddy-driven Ferrel circulation at mid latitudes of the Earth's troposphere, which derives its motion by converting the kinetic energy of the motion into potential energy, is absent on Titan. In fact, the role of heat transport by baroclinic eddies seems to be minimal on Titan, because the favored scale for energy conversion by the eddies, the Rossby radius of deformation, is much larger than Titan's radius (Leovy and Pollack 1973; Flasar et al. 1981; Hunten et al. 1984; Flasar 1998b).

There is little doubt that a Hadley circulation exists and transports heat meridionally in the lower atmosphere. The observed equator-to-pole thermal contrasts are much smaller than those expected if only radiative processes operated (Section 13.3.1). The need for meridional heat transport is also indicated by the imbalance seen in the radiative flux measurements by the Huygens DISR. These indicate that the solar heating rate at the landing site (10°S) is significantly larger than the thermal cooling rate in the entire lower atmosphere (Tomasko et al. 2008). Because of the expected seasonal variations in surface temperatures and the surface coupling via convection to the overlying atmosphere (Section 13.2), the Hadley cells cannot be expected to be symmetric about the equator except at limited times. When the location of maximum solar heating is off the equator the latitude of the boundary between the summer and winter Hadley cell (i.e., the intertropical convergence zone, ITCZ) has to be poleward of the latitude of maximum solar heating in order to ensure continuity of temperature and conservation of energy across this boundary (Lindzen and Hou 1988). This was indeed numerically shown by parametric GCM simulations of Williams (1988), who concluded that on Titan, which is characterized by a slow rotation and medium obliquity, the circulation should vary from the symmetric Hadley state at equinox to the solstitial-symmetric Hadley state with a single pole-to-pole cell at solstice.

Numerical modeling has provided a more complete picture of meridional circulation and its seasonal modulation, albeit with uncertainties because of the limited data available. The first Titan GCM with realistic radiative forcing and planetary parameters of Titan was developed by Hourdin et al. (1995). This 3-dimensional model is based on so-called primitive equations, which are Navier-Stokes equations of hydrodynamics in which the vertical momentum equation is replaced by the hydrostatic approximation and a few small terms in the horizontal momentum equations are neglected to ensure angular momentum conservation. The radiative forcing was calculated with the radiation model of McKay et al. (1989), which as a radiative-convective model reproduced the vertical temperature profile retrieved from the Voyager data. The predicted mean meridional circulation cell covered almost the entire globe, i.e., there is a single pole-to-pole cell with ascent near the spring and summer pole and subsidence near the autumn and winter pole. When the season approaches the equinox, a reversal of the Hadley cell takes place during which temporarily two equator-to-pole cells exist. Other GCMs that use the same radiation model (Tokano et al. 1999; Richardson et al. 2007; Friedson et al. 2008) essentially reproduce the same meridional circulation pattern and seasonal reversal. The mass stream function peaks near the surface at ~$10^{10}$ kg $s^{-1}$ in either model, indicating that the majority of meridional mass transport takes place in the lower troposphere. Figure 13.12 gives an illustrative example.

Given the presence of an Earth-like hydrology based on methane on Titan and the importance of the water cycle on Earth's climate, it is intuitive to expect a significant impact of methane hydrology on Titan's atmospheric circulation. However, GCMs that include methane condensation (Tokano et al. 2001; Rannou et al. 2006; Mitchell et al. 2006) have so far yielded conflicting interpretations as to the role of methane on the general circulation. Radiative effects of gaseous and condensed methane and latent heat effects have been sometimes included, but presently, models that do not include methane condensation in the troposphere seem to predict more realistic circulation patterns (Tokano 2008b), indicating that either methane hydrology is not relevant for the general circulation or else it is not yet well understood.

Although eddy-driven thermally indirect circulations, like the terrestrial Ferrel cell, are unlikely on Titan, this does not mean that thermally indirect circulations do not exist, at least locally, in the middle atmosphere. The likely subsidence over the warm winter north polar stratopause, leading to an enhancement of several organic compounds at a given altitude, has already been discussed (Sections 13.4.1 and 13.4.2). Earth's warm mesopause is another example of a thermally indirect circulation, and it is likely forced by the interaction of the mean zonal flow with vertically propagating waves (see, e.g., Andrews et al. 1987). The fact that Titan's zonal wind profile (Fig. 13.2) decays with altitude above the 0.1-mbar level indicates that the flow is being damped, and waves – perhaps internal gravity waves – are a likely candidate, as they are on Earth. The zonally symmetric circulation proposed by Flasar and Conrath (1990, see Section 13.4.2) to explain the lag in cooling of the stratosphere in the summer hemisphere, as it moved into autumn, is another example of a thermally indirect flow.

Uncorrected Proof

### 13.7.2 Zonal Circulation and Superrotation

In the Earth's atmosphere the zonal wind is strongly coupled to the meridional wind via the Coriolis force and is in geostrophic wind balance. The angular momentum transport by the Hadley circulation at low latitudes and in the polar region as well as by baroclinic instability at mid latitudes basically determines the global zonal wind pattern. On the other hand, the small Coriolis parameter and the lack of baroclinic instability on Titan imply that the global zonal wind pattern is likely to be governed by another force balance and another type of angular momentum redistribution. Titan's zonal circulation is in cyclostrophic wind balance everywhere above the upper troposphere, but the winds generally decrease with decreasing altitude, and in the lower troposphere there is a transition to Earth-like geostrophic wind balance (Tokano 2007).

A fundamental question of Titan's general circulation is as to how superrotating winds can be maintained in the entire stratosphere including the equatorial region, when the maximum angular momentum/mass ($m$) in a purely axisymmetric circulation cannot exceed that of the equatorial surface (Hide 1969; see also Held and Hou 1980). Jets at mid or high latitudes can be generated by poleward transport of angular momentum by the mean meridional circulation, but such momentum transport would also cause easterlies at the equator as on Earth in the absence of some counter-gradient transport of momentum by eddies. Basic concepts of superrotation formation mechanism (proposed for Venus) can be broadly subdivided into those which rely on the day–night circulation, gravity waves, and mean meridional circulation with horizontal mixing (Gierasch et al. 1997).

Gierasch (1975) proposed a model to explain the maintenance of the superrotation of the Venusian atmosphere that has also been considered in the discussion of Titan's atmospheric superrotation. It involves Hadley cells with ascent at the equator, consistent with the maximum solar heating there, and subsidence at the poles. The zonal winds increase with altitude, and the specific angular momentum ($m$) is greatest at the equator, where the lever arm to the rotation axis is largest. (It is hard to imagine a configuration where $m$ increases with latitude. Were it to increase with latitude along isentropes, which are nearly horizontal, inertial instability would result (see, e.g., Held and Hou 1980). The Hadley circulation carries atmosphere with high $m$ upward at low latitudes. The atmosphere in the upper leg of the circulation moves poleward and tends to conserve angular momentum, spinning up and forming jets at high latitudes. These jets can become barotropically unstable because of the large horizontal shear of the wind near the jet core. Barotropic eddies arising in this area efficiently transport angular momentum back towards the equator, thereby maintaining a steady balance with equatorial superrotation. There are several necessary requirements for this idealized mechanism to work: the zonal wind must be strong enough for cyclostrophic balance, vertical mixing of momentum must be slower than meridional overturning, and meridional mixing by eddies must be faster than meridional overturning.

Prior to the advent of Titan's wind data, GCMs were the only means of investigating this hypothesis for Titan's atmosphere. When a terrestrial GCM is run at Titan's slow rotation rate, all other parameters being unchanged, the Hadley circulation becomes wider in meridional extent and the zonal wind tends to superrotate, provided turbulent coupling of the atmosphere aloft with the surface is weak (Del Genio et al. 1993). This is possible when much of the solar heating occurs aloft, far removed from the surface, as it does in Venus's clouds and Titan's hazes. An analysis of the angular momentum cycle in that GCM confirmed that the Gierasch mechanism could indeed work under Titan's rotation rate. However, if Titan's Hadley circulation is not symmetric about the equator because of the seasonal migration in response to solar heating, the upwelling region of the Hadley circulation will often not be located near the equator, where the angular momentum of the atmosphere is largest. Therefore, it is insufficient to change only the rotation rate or other geophysical parameters such as planetary radius in the GCM, but importantly a realistic diabatic heating pattern as a driver of the mean meridional circulation is necessary.

The Titan GCM of Hourdin et al. (1995) predicted a slow spin-up of the stratospheric superrotation over a period of 30 Titan years (900 years), causing zonal winds of up to 120 m $s^{-1}$ in the upper stratosphere including the equatorial region. Hourdin et al. (1995) ascribed the build-up of the superrotation to the Gierasch mechanism. In their model there was an annual mean approximate balance between the net upward transport of angular momentum by the Hadley circulation and downward diffusion of the angular momentum, although upward transport slightly prevailed during the entire simulation period. However, since the ascending branch of the Hadley circulation on Titan is located near the summer poles during most of the Titan year, angular momentum is not efficiently carried into the stratosphere except during the relatively short reversal of the Hadley circulation near the equinoxes, when the ascending branch moves across the equator.

However, the result of Hourdin et al. (1995) and the Gierasch mechanism are not universally reproduced in other Titan GCMs. Tokano et al. (1999) predicted very weak zonal winds in the entire atmosphere although the same radiation model was used and the calculated meridional circulation resembled that of Hourdin et al. (1995). The meridional heat transport by the Hadley circulation was so efficient that the meridional temperature gradient almost disappeared and was in thermal wind balance with the weak zonal wind. Similar results were also predicted by Friedson et al. (2008), using a GCM, and by Zhu and Strobel (2005a), using a 2-dimensional dynamics model. Another similar GCM of Richardson

Uncorrected Proof

et al. (2007) predicted a similar, almost vanishing, meridional temperature gradient, but the zonal wind attained a maximum of 30 m $s^{-1}$, stronger than in Tokano et al. (1999) but substantially weaker than predicted by Hourdin et al. (1995) and observed by Huygens. The reason for the large discrepancies among the 3-dimensional GCMs is not understood.

Tokano and Neubauer (2002) have pointed out that the inclusion of Saturn's gravitational tide in the GCM works against the maintenance of strong superrotation, since the breaking of the tide in the stratosphere decelerates the zonal wind towards the phase speed of the tide, which is only 6 m $s^{-1}$ at the equator. This indicates that a forcing mechanism of superrotation would have to exist that overcomes this deceleration in the upper stratosphere.

Since absorption of sunlight by the stratospheric haze is the major heat source in the stratosphere, one anticipates that seasonal transport of haze particles from hemisphere to hemisphere by the Hadley circulation would affect the heating pattern, meridional circulation and temperature. This effect was first taken into account by Rannou et al. (2004) in a 2-dimensional GCM coupled to haze microphysics and photochemistry. In these models, the effects of barotropic eddies were parameterized (Luz et al. 2003). The meridional circulation tends to accumulate the haze particles in the polar region, enhancing the thermal cooling particularly at the winter pole. This lowers the winter pole temperature, in agreement with observation, and simultaneously enhances the zonal wind in the winter hemisphere in response to a larger meridional temperature gradient. In this and subsequent model versions the predicted zonal wind and temperature in the stratosphere are generally in close agreement to the Cassini temperature and wind data (Crespin et al. 2008). However, the tropospheric wind in their GCMs is up to twice as strong as measured by Huygens. As a whole, current major Titan GCMs are faced with the peculiar situation in which one series of GCMs predicts realistic superrotation that is in balance with unrealistic, excessive tropospheric winds (Rannou et al. 2004; Crespin et al. 2008), while another series predicts realistic tropospheric winds in balance with unrealistic, negligible superrotation (Tokano et al. 1999; Tokano 2007). This may indicate the presence of additional mechanisms relevant for the superrotation that are not adequately modeled.

An adaptation of the Gierasch model has been invoked to explain the origin of the curious 4° pole tilt in the temperatures and zonal winds reported by Achterberg et al. (2008b) (Section 13.3.1). As noted above, the most favorable configuration for transporting angular moment upward by an axisymmetric circulation is with ascent at the equator. However, the thermally direct Hadley cells transport heat most efficiently with ascent below the subsolar point. Achterberg et al. speculate that the tilt represents a compromise, with the spin equator shifting toward the sun. They use a simple toy model with several frictionally coupled spherical shells of atmosphere. Imposing a vertical motion field, corresponding to a fixed meridional circulation, they follow the evolution of the spin axis of the top shell relative to the surface rotation. The model shows the spin equator of the shell tilting toward the sun, with the spin axis lagging (on seasonal time scales) the direction to the sun as observed. It predicts that the pole tilt should follow the sun, with a lag, and this should be detectable given observations over seasonal time scales. Because of the strong frictional coupling troposphere to the surface (Section 13.5), it follows that the 4° offset cannot persist at all altitudes, but must decrease through the lower atmosphere.

Another mechanism for generating equatorial superrotation involves direct forcing by waves. Forcing by thermal tides has been proposed to account for Venus's superrotation (see, e.g., Pechmann and Ingersoll 1984; Leovy 1987; Gierasch et al. 1997). Thermal tides have long been considered negligible on Titan given the relatively weak solar heating rate and the long radiative time constants compared to the diurnal cycle (Flasar 1998b; Section 13.2). More recently, Zhu (2006) performed a scale analysis of the momentum equations for Titan's atmosphere and showed that there is a balance between the zonal momentum pumping by thermal tides and frictional drag if the main solar heating layer is located near 300 km. However, no strong zonal variation in the upper stratospheric temperatures has been observed (at least about the tilted pole, Section 13.3.1) in the nadir-viewing data, which provides the most complete zonal coverage (Teanby et al. 2006; Achterberg et al. 2008). Note that the [AU12]
vertical resolution of the nadir observations is comparable to a pressure scale height, $H$; waves with vertical wavenumbers $m$, such that $mH >> 1$, would be averaged out in the retrievals. Vertically propagating internal gravity waves offers another possibility. In Venus' atmosphere Hou and Farrell (1987) have proposed absorption of vertically propagating gravity waves as a mechanism for maintaining cyclostrophic winds below the clouds. Scintillations in Voyager radio-occultation profiles have led to the identification of small-scale gravity waves in Titan's stratosphere (Hinson and Tyler 1983), as noted earlier.

## 13.8 Key Questions and Future Prospects

Even though it is cyclostrophic, Titan's middle atmosphere exhibits a dynamical behavior that shares a lot of common ground with that of Earth, which is geostrophic. This includes:

- Strong seasonal behavior with cross-hemispheric transport
- A strong circumpolar vortex in the winter hemisphere that acts to isolate the enclosed air mass
- Anomalous concentrations of gases within the vortex
- Stratospheric condensate clouds within the vortex

Uncorrected Proof

Yet a lot is still elusive:

- Is heterogeneous chemistry, involving stratospheric condensates, important, as it is on Earth?
- What physical, chemical, and dynamical processes are important in the mesosphere above 400 km, a region that has had only limited sounding.
- How does the vortex break up, as it must, when the winter hemisphere moves into summer?
- What drives the global superrotation?

On Earth planetary waves disrupt the winter polar vortex as it weakens in late spring. The disruption is nonlinear, with the waves producing large distortions in the vortex itself. Planetary-scale waves have yet to be identified on Titan, so it is not obvious if its winter vortices will break up so spectacularly, or if they will simply fade away, perhaps a victim of small-scale erosion by turbulence and waves.

The meteorology of Titan's troposphere is a little more mysterious. In part, this is because it is harder to probe than the middle atmosphere via remote sensing, because of the enshrouding photochemical smog. This not only makes observations that can probe the troposphere more difficult to conceive, but can also complicate the analysis of observations that do. Terrestrial analogies are still present:

- A hydrological cycle ($CH_4$), although with lakes and not oceans
- Hadley circulations as a fundamental engine for redistributing heat and angular momentum
- Changes in the length of day from angular momentum transfers between the atmosphere and the surface

There are several unanswered questions in tropospheric meteorology. A few:

- Do the "lakes" of liquefied natural gas migrate seasonally?
- Does moist convection play an important role in the energy and momentum budget, as it does on Earth?
- What role does topography play in the circulation and meteorology, e.g., in forcing atmospheric waves?

There are also major differences between Titan's atmosphere and Earth's. Titan has a major gravitational tidal perturbation from Saturn's mass and proximity. Titan's circulation seems to be axisymmetric, but with significant pole tilts aloft. Is this a property of seasonally modulated cyclostrophic systems?

The highlights and questions above are not meant to be exhaustive, but they indicate two tacks that one needs to take in pursuing Titan dynamical studies. The first is that time is an important dimension to map out, in additional to spatial dimensions. Dynamical systems change, and that change is instructive, particularly if it is unanticipated. No one would have predicted, much less explained, the Antarctic ozone hole on Earth, for example, without repeated observations that extended over several years. The interaction of physics, chemistry, and dynamics turned out to be fairly complex. Titan also has an annual cycle. Planetary scientists have known of Venus's global superrotation for decades, yet there is no completely satisfactory theory of how it originated and is maintained. Titan is the second solar-system body with a superrotating atmosphere, and it brings the seasonality that Venus lacks to the analyst's table. Observing the change with seasons may provide the missing clues needed to unravel this puzzle. Titan may have longer-term cycles analogous to those on Earth, like the El Niño Southern Oscillation. Of course, this example involves ocean currents and variability in sea-surface temperatures, and oceans on Titan seem to be nonexistent, but that is not the point. What the study of Earth's atmosphere has taught everyone is that the range of physical phenomena is rich and diverse. There is no reason to think things are different on Titan. One has to show up and observe.

The second aspect is that observations different from those previously done need to be made. For a remote body, this becomes tricky: one cannot just launch a rocket from the surface or send up a tethered balloon, each laden with instruments, as has been done on Earth. But ultimately more in situ sounding will need to be done. There are limits to what remote sensing can accomplish.

Several studies of the next flagship mission to Titan, which variously include an orbiter, a balloon, and some kind of surface probe, can begin to address these issues. And the current good health of Cassini and prospects for extending its mission beyond the current Equinox Mission (ends 2010) is an important factor. Keeping in mind the length of Titan's year, it is clear that no single mission will answer all the questions that have been posed, and that a series of missions will ultimately be needed. One needs to keep a long-term view.

Uncorrected Proof

## References [AU13]

Achterberg RK, Conrath BJ, Gierasch PJ, Flasar FM, Nixon CA (2008a) Titan's middle-atmospheric temperatures and dynamics observed by the Cassini composite infrared spectrometer. Icarus 194:263–277. doi:10.1016/j.icarus.2007.09.029

Achterberg RK, Conrath BJ, Gierasch PJ, Flasar FM, Nixon CA (2008b) [AU14] Observation of a tilt of titan's middle-atmospheric superrotation. Icarus. doi:10.1016/j.icarus.2008. 05.014 (in press)

Andrews DG, Holton JR, Leovy CB (1987) Middle atmosphere dynamics. Academic, Orlando

Atkinson DH (1989) Measurement of planetary wind fields by Doppler monitoring of an atmospheric entry vehicle. Ph.D. Thesis. Washington State University, Pullman, WA

Atkinson DH, Pollack JB, Seiff A (1990) Measurement of a zonal wind profile on Titan by Doppler tracking of the Cassini entry probe. Radio Sci 25:865–882

Atkinson DH, Kazeminejad B, Lebreton J-P, Witasse O, Pérez-Ayúcar M, Matson DL (2007) The Huygens probe descent trajectory working group: organizational framework, goals, and implementation. Planet Space Sci 55:1877–1885

Awal M, Lunine JI (1994) Moist convective clouds in Titan's atmosphere. Geophys Res Lett 21:2491–2494

Baines KH, Drossart P, Momary TW, Formisano V, Griffith C, Bellucci G, Bibring J-P, Brown R.H, Buratti BJ, Capaccioni F, Cerroni P, Clark RN, Coradini A, Cruikshank DP, Jaumann R, Langevin Y, Matson DL, McCord TB, Mennella V, Nelson RM, Nicholson PD, Sicardy B, Sotin C (2005) The atmospheres of Saturn and Titan in the near-infrared: first results of Cassini/VIMS. Earth Moon Planets 96:119–147

Barth EL, Rafkin SCR (2007) TRAMS: a new dynamic cloud model for Titan's methane. Geophys Res Lett 34:L03203

Bézard B, Coustenis A, McKay CP (1995) Titan's stratospheric temperature asymmetry: a radiative origin? Icarus 113:267–276

Bird MK, Heyl M, Allison M, Asmar SW, Atkinson DH, Edenhofer P, Plettemeier D, Wohlmuth R, Iess L, Tyler GL (1997) The Huygens doppler wind experiment. In: Huygens science payload and mission, ESA SP-1177:139–162

Bird MK, Allison M, Asmar SW, Atkinson DH, Avruch IM, Dutta-Roy R, Dzierma Y, Edenhofer P, Folkner WM, Gurvits LI, Johnston DV, Plettemeier D, Pogrebenko SV, Preston RA, Tyler GL (2005) The vertical profile of winds on Titan. Nature 438:800–802

[AU15] Bouchez AH (2003) Seasonal trends in Titan's atmosphere: haze, wind, and clouds. Ph. D. Thesis. California Institute of Technology. http://resolver.caltech.edu/CaltechETD:etd-10272003-092206

Bouchez AH, Brown ME (2005) Statistics of Titan's south polar tropospheric clouds. Astrophys J 618:L53–L56

Brown ME, Bouchez AH, Griffith CA (2002) Direct detection of variable tropospheric clouds near Titan's South Pole. Nature 420:795–797

Brown RH, Baines KH, Bellucci G, Buratti BJ, Capacionni F, Cerroni P, Clark RN, Coradini A, Cruikshank DP, Drossart P, Formisano V, Jaumann R, Langevin Y, Matson DL, McCord TB, Mennella V, Nelson RM, Nicholson PD, Sicardy B, Sotin C, Baugh N, Griffith C, Hansen G, Hibbitts K, Showalter MR (2006) Observations in the Saturn system during approach and orbital insertion, with Cassini's visual and infrared mapping spectrometer (VIMS). Astron Astrophys 446:707–716

Chapman S, Lindzen RS (1970) Atmospheric tides. Reidel, Dordrecht

Colombatti G, Withers P, Ferri F, Aboudan A, Ball AJ, Bettanini C, Gaborit V, Harri AM, Hathi B, Leese MR, Makinen T, Stoppato PL, Towner MC, Zarnecki JC, Angrilli F, Fulchignoni M (2008) Reconstruction of the trajectory of the Huygens probe using the Huygens atmospheric structure instrument (HASI). Planet Space Sci 56:586–600

Counselman CC III, Gourevitch SA, King RW, Loriot GB, Ginsberg ES (1980) Zonal and meridional circulation of the lower atmosphere of Venus determined by radio interferometry. J Geophys Res 85:8026–8030

Crespin A, Lebonnois S, Vinatier S, Bézard B, Coustenis A, Teanby NA, Achterberg RK, Rannou P, Hourdin F (2008) Diagnostics of Titan's stratospheric dynamics using Cassini/CIRS data and the 2-dimensional IPSL circulation model. Icarus 192(2):556–571. doi:10.1016/j.icarus.2008.05.010

Del Genio AD, Zhou W, Eichler TP (1993) Equatorial superrotation in a slowly rotating GCM: implications for Titan and Venus. Icarus 101:1–17

Dunkerton T (1978) On the mean meridional mass motions of the stratosphere and mesosphere. J Atmos Sci 35:2325–2333

Dutta-Roy R, Bird MK (2004) The Huygens doppler wind experiment: a Titan zonal wind retrieval algorithm. In: Planetary probe atmospheric entry and descent trajectory analysis and science, ESA SP-544:109–116

Dzierma Y, Bird MK, Dutta-Roy R, Perez-Ayucar M, Plettemeier D, Edenhofer P (2007) Huygens probe descent dynamics inferred from channel B signal level measurements. Planet Space Sci 55:1886–1895

Flasar FM (1983) Oceans on Titan? Science 221:55–57

Flasar FM (1998a) The composition of Titan's atmosphere: a meteorological perspective. Planet Space Sci 46:1109–1124

Flasar FM (1998b) The dynamic meteorology of Titan. Planet Space Sci 46:1125–1147

Flasar FM, Achterberg RK (2009) The structure and dynamics of Titan's middle atmosphere. Phil Trans Roy Soc London 367:649–664

Flasar FM, Conrath BJ (1990) Titan's stratospheric temperature: a case for dynamical inertia? Icarus 85:346–354

Flasar FM, Samuelson RE, Conrath BJ (1981) Titan's atmosphere: temperature and dynamics. Nature 292:693–698

Flasar FM, Allison M, Lunine JI (1997) Titan zonal wind model. In: Huygens science payload and mission, ESA SP-1177:287–298

Flasar FM, Kunde VG, Abbas MM, Achterberg RK, Ade P, Barucci A, Bézard B, Bjoraker GL, Brasunas JC, Calcutt S, Carlson R, Césarsky CJ, Conrath BJ, Coradini A, Courtin R, Coustenis A, Edberg S, Edgington S, Ferrari C, Gautier D, Gierasch PJ, Grossman K, Irwin P, Jennings DE, Lellouch E, Mamoutkine AA, Marten A, Meyer JP, Nixon CA, Orton GS, Owen TC, Pearl JC, Prangé R, Raulin F, Read PL, Romani PN, Samuelson RE, Segura ME, Showalter MR, Simon-Miller AA, Smith MD, Spencer JR, Spilker LJ, Taylor FW (2004) Exploring the Saturn system in the thermal infrared: the composite infrared spectrometer. Space Sci Rev 115:169–297

Flasar FM, Achterberg RK, Conrath BJ, Gierasch PJ, Kunde VG, Nixon CA, Bjoraker GL, Jennings DE, Romani PN, Simon-Miller AA, Bézard B, Coustenis A, Irwin PGJ, Teanby NA, Brasunas JC, Pearl JC, Segura ME, Carlson RC, Mamoutkine AA, Schinder PJ, Barucci A, Courtin R, Fouchet T, Gautier D, Lellouch E, Marten A, Prangé R, Vinatier S, Strobel DF, Calcutt SB, Read PL, Taylor FW, Bowles N, Samuelson RE, Orton GS, Spilker LJ, Owen TC, Spencer JR, Showalter MR, Ferrari C, Abbas MM, Raulin F, Edgington S, Ade P, Wishnow EH (2005) Titan's atmospheric temperatures, winds, and composition. Science 308:975–978

Folkner WM, Preston RA, Border JS, Navarro J, Wilson WE, Oestreich M (1997) Earth-based radio tracking of the Galileo Probe for Jupiter wind estimation. Science 275:644–646

Folkner WM, Border JS, Lowe ST, Preston RA, Bird MK (2004) Ground-based tracking of the Huygens Probe during the Titan descent. In: Planetary probe atmospheric entry and descent trajectory analysis and science, ESA SP-544:191–196

Folkner WM, Asmar SW, Border JS, Franklin GW, Finley SG, Gorelik J, Johnston DV, Kerzhanovich VV, Lowe ST, Preston RA, Bird MK, Dutta-Roy R, Allison M, Atkinson DH, Edenhofer P. Plettemeier D, Tyler GL (2006) Winds on Titan from ground-based tracking of the Huygens probe. J Geophys Res 111:E07S02

Friedson AJ, West RA, Wilson EH, Oyafuso F, Orton GS (2008) A global climate model of Titan's atmosphere and surface. In preparation [AU16]

Fulchignoni M, Ferri F, Angrilli F, Ball AJ, Bar-Nun A, Barucci MA, Bettanini C, Bianchini G, Borucki W, Colombatti G, Coradini M, Coustenis A, Debei S, Falkner P, Fanti G, Flamini E, Gaborit V, Grard R, Hamelin M, Harri AM, Hathi B, Jernej I, Leese MR, Lehto A, Lion Stoppato PF, López-Moreno JJ, Mäkinen T, McDonnell JAM, McKay CP, Molina-Cuberos G, Neubauer FM, Pirronello V, Rodrigo R, Saggin B, Schwingenschuh K, Seiff A, Simões F, Svedhem H, Tokano T, Towner MC, Trautner R, Withers P, Zarnecki JC (2005) Titan's physical characteristics measured by the Huygens atmospheric structure instrument (HASI). Nature 438:785–791

Gibbard SG, Macintosh B, Gavel D, Max CE, de Pater I, Roe HG, Ghez AM, Young EF, McKay CP (2004) Speckle imaging of Titan at 2 microns: surface albedo, haze optical depth, and tropospheric clouds 1996–1998. Icarus 169:429–439

Gierasch PJ (1975) Meridional circulation and the maintenance of the Venus atmospheric rotation. J Atmos Sci 32:1038–1044

Gierasch PJ, Goody RM, Young RE, Crisp D, Edwards C, Kahn R, Rider D, Del Genio A, Greeley R, Hou A, Leovy CB, McCleese D, Newman M. (1997) The general circulation of the Venus atmosphere: An assessment. In: Bougher SW, Hunten DM, Phillips RJ (eds) Venus II. University of Arizona Press, Tucson, AZ, pp 459–500

Uncorrected Proof

Griffith CA, Hall JL, Geballe TR (2000) Detection of daily clouds in Titan. Science 290:509–513

Griffith CA, Penteado P, Baines K, Drossart P, Barnes J, Bellucci G, Bibring J, Brown R, Buratti B, Capaccioni F, Cerroni P, Clark R, Combes M, Coradini A, Cruikshank D, Formisano V, Jaumann R, Langevin Y, Matson D, McCord T, Mennella V, Nelson R, Nicholson P, Sicardy B, Sotin C, Soderblom LA, Kursinski R (2005) The evolution of Titan's mid-latitude clouds. Science 310:474–477

Held IM, Hou AY (1980) Nonlinear axially symmetric circulations in a nearly inviscid atmosphere. J Atmos Sci 37:515–533

Hide R (1969) The viscous boundary layer at the rigid bounding surface of an electrically-conducting rotating fluid in the presence of a magnetic field. J Atmos Sci 26:847–853

Hinson DP, Tyler GL (1983) Internal gravity waves in Titan's atmosphere observed by Voyager radio occultation. Icarus 54:337–352

Hirtzig M, Coustenis A, Gendron E, Drossart P, Negrão A, Combes M, Lai O, Rannou P, Lebonnois S, Luz D (2006) Monitoring atmospheric phenomena on Titan. Astron Astroph 456:761–774

Holton JR (1979) An introduction to dynamic meteorology, 2nd edn. Academic, New York

Hou AY, Farrell BF (1987) Superrotation induced by critical-level absorption of gravity waves on Venus: an assessment. J Atmos Sci 44:1049–1061

Hourdin F, Talagrand O, Sadourny R, Courtin R, Gautier D, McKay CP (1995) Numerical simulation of the general circulation of the atmosphere of Titan. Icarus 117:358–374

Hourdin F, Lebonnois S, Luz D, Rannou P (2004) Titan's stratospheric composition driven by condensation and dynamics. J Geophys Res 109:E12005. doi:10.1029/2004JE002282

Hubbard WB, Sicardy B, Miles R, Hollis AJ, Forrest RW, Nicolson IKM, Appleby G, Beisker W, Bittner C, Bode H-J, Bruns M, Denzau H, Nezel M, Riedel E, Struckmann H, Arlot JE, Roques F, Sevre F, Thuillot W, Hoffmann M, Geyer EH, Buil C, Colas F, Lecacheux J, Klots A, Thouvenot E, Vidal JL, Carreira E, Rossi F, Blanco C, Cristaldi S, Nevo Y, Reitsema HJ, Brosch N, Cernis K, Zdanavicius K, Wasserman LH, Hunter DM, Gautier D, Lellouch E, Yelle RV, Rizk B, Flasar FM, Porco CC, Toublanc D, Corugedo G (1993) The occultation of 28 Sgr by Titan. Astron Astrophys 269:541–563

Hueso R, Sánchez-Lavega A (2006) Methane storms on Saturn's moon Titan. Nature 442:428–431

Hunten DM, Tomasko MG, Flasar FM, Samuelson RE, Strobel DF, Stevenson DJ (1984) Titan. In: Gehrels T, Matthews M (eds) Saturn. University of Arizona Press, Tucson, pp 671–759

Karatekin Ö, Van Hoolst T (2006) The effect of a dense atmosphere on the tidally induced potential of Titan. Icarus 183:230–232

Karkoschka E, Lorenz RD (1997) Latitudinal variation of aerosol sizes inferred from Titan's shadow. Icarus 125:369–379

Karkoschka E, Tomasko MG, Doose LR, See C, McFarlane EA, Schröder SE, Rizk B (2007) DISR imaging and the geometry of the descent of the Huygens probe within Titan's atmosphere. Planet Space Sci 55:1896–1935

Kazeminejad B, Atkinson DH, Pérez-Ayúcar M, Lebreton J-P, Sollazzo C (2007) Huygens' entry and descent through Titan's atmosphere: methodology and results of the trajectory reconstruction. Planet Space Sci 55:1845–1876

Kostiuk T, Fast KE, Livengood TA, Hewagama T, Goldstein JJ, Espenak F, Buhl D (2001) Direct measurement of winds on Titan. Geophys Res Lett 28:2361–2364

Kostiuk T, Livengood TA, Hewagama T, Sonnabend G, Fast KE, Murakawa K, Tokunaga AT, Annen J, Buhl D, Schmülling F (2005) Titan's stratospheric zonal wind, temperature and ethane abundance a year prior to Huygens insertion. Geophys Res Lett 32:L22205

Kostiuk T, Livengood TA, Sonnabend G, Fast KE, Hewagama T, Murakawa K, Tokunaga AT, Annen J, Buhl D, Schmülling F, Luz D, Witasse O (2006) Stratospheric global winds on Titan at the time of the Huygens descent. J Geophys Res 111:E07S03

Lellouch E, Coustenis A, Gautier D, Raulin F, Dubouloz N, Frére C (1989) Titan's atmosphere and hypothesized ocean: a reanalysis of the Voyager 1 radio-occultation and IRIS 7.7 μm data. Icarus 79:328–349

Leovy CB (1973) Rotation of the upper atmosphere of Venus. J Atmos Sci 30:1218–1220

Leovy CB (1987) Zonal winds near Venus' cloud top level: an analytic model of the equatorial wind speed. J Atmos Sci 69:193–201

Leovy CB, Pollack JB (1973) A first look at atmospheric dynamics and temperature variations on Titan. Icarus 19:195–201

Lindal GF, Wood GE, Hotz HB, Sweetnam DN, Eshleman V, Tyler GL (1983) The atmosphere of Titan: an analysis of the Voyager 1 radio occultation measurements. Icarus 53:348–363

Lindzen RS, Hou AY (1988) Hadley circulations for zonally averaged heated centered off the equator. J Atmos Sci 42:2416–2427

Lorenz RD (1993) The life, death, and afterlife of a raindrop on Titan. Planet Space Sci 41:647–655

Lorenz RD (2006) Thermal interactions of the Huygens probe with the Titan environment: constraints on near-surface wind. Icarus 182:559–566

Lorenz RD, McKay CP (2003) A simple expression for vertical convective fluxes in planetary atmospheres. Icarus 165:407–413

Lorenz RD, Smith PH, Lemmon MT, Karkoschka E, Lockwood GW, Caldwell J (1997) Titan's north–south asymmetry from HST and voyager imaging: comparison with models and ground-based photometry. Icarus 127:173–189

Lorenz RD, Griffith CA, Lunine JI, McKay CP, Rennò NO (2005) Convective plumes and the scarcity of Titan's clouds. Geophys Res Lett 32:L01201

Lorenz RD, Wall S, Radebaugh J, Boubin G, Reffet E, Janssen M, Stofan E, Lopes R, Kirk R, Elachi C, Lunine J, Mitchell K, Paganelli F, Soderblom L, Wood C, Wye L, Zebker H, Anderson Y, Ostro S, Allison M, Boehmer R, Callahan P, Encrenaz P, Ori GG, Francescatti G, Gim Y, Hamilton G, Hensley G, Johnson W, Kelleher K, Muhleman D, Picardi G, Posa F, Roth L, Seu R, Shaffer S, Stiles B, Vetralla S, Flamini E, West R (2006) The sand seas of Titan: Cassini RADAR observations of longitudinal dunes. Science 312:724–727

Lorenz RD, Zarnecki JC, Towner MC, Leese MR, Ball AJ, Hathi B, Hagermann A, Ghafoor NAL (2007) Descent motions of the Huygens probe as measured by the surface science package (SSP): turbulent evidence for a cloud layer. Planet Space Sci 55: 1936–1948

Lorenz RD, Stiles BW, Kirk RL, Allison MD, Persi del Marmo P, Iess L, Lunine JI, Ostro SJ, Hensley S (2008) Titan's rotation reveals an internal ocean and changing zonal winds. Science 319:1649–1651

Lorenz RD, Brown ME, Flasar FM (2009) Seasonal change on Titan. In: Brown RH, Lebreton J-P, Waite JH (eds) Titan after Cassini-Huygens. Springer [AU17]

Lunine JI, Atreya SK (2008) The methane cycle on Titan. Nature Geosci 1:159–164

Luz D, Hourdin F, Rannou P, Lebonnois S (2003) Latitudinal transport by barotropic waves in Titan's stratosphere. II. Results from a coupled dynamics-microphysics-photochemistry GCM. Icarus 166: 343–358

Luz D, Civeit T, Courtin R, Lebreton J-P, Gautier D, Rannou P, Kaufer A, Witasse O, Lara L, Ferri F (2005) Characterization of zonal winds in the stratosphere of Titan with UVES. Icarus 179:497–510

Luz D, Civeit T, Courtin R, Lebreton J-P, Gautier D, Witasse O, Kaufer A, Ferri F, Lara L, Livengood T, Kostiuk T (2006) Characterization of zonal winds in the stratosphere of Titan with UVES: 2. Observations coordinated with the Huygens probe entry. J Geophys Res 111:E08S90

Mäkinen JTT, Harri A-M, Tokano T, Savijärvi H, Siili T, Ferri F (2006) Vertical atmospheric flow on Titan as measured by the HASI instrument on board the Huygens probe. Geophys Res Lett 33:L21803

McKay CP, Pollack JB, Courtin R (1989) The thermal structure of Titan's atmosphere. Icarus 80:23–53

Uncorrected Proof

McKay CP, Pollack JB, Courtin R (1991) The greenhouse and antigreenhouse effects on Titan. Science 253:1118–1121

Mitchell JL (2008) The drying of Titan's dunes: Titan's methane hydrology and its impact on atmospheric circulation. J Geophys Res 113:E08105

Mitchell JL, Pierrehumbert RT, Frierson DMW, Caballero R (2006) The dynamics behind Titan's methane clouds. Proc Natl Acad Sci USA 103:18421–18426

Mitri G, Showman AP, Lunine JI, Lorenz RD (2007) Hydrocarbon lakes on Titan. Icarus 186:385–394

Moreno R, Marten A, Hidayat T (2005) Interferometric measurements of zonal winds on Titan. Astron Astrophys 437:319–328

Pechmann JB, Ingersoll AP (1984) Thermal tides in the atmosphere of Venus: comparison of model results with observations. J Atmos Sci 41:3290–3313

[AU18] Pentaedo PF, Griffith CA, Tomasko MG, Engel S, See C, Doose L (2008) Latitudinal variations in Titan's methane and haze from Cassini VIMS observations. Icarus (submitted)

Pogrebenko SV, Gurvits LI, Campbell RM, Avruch IM, Lebreton J-P, van't Klooster CGM (2004) VLBI tracking of the Huygens probe in the atmosphere of Titan. In: Planetary probe atmospheric entry and descent trajectory analysis and science, ESA SP-544: 197–204

Porco CC, Baker E, Barbara J, Beurle K, Brahic A, Burns JA, Charnoz S, Cooper N, Dawson D, Del Genio AD, Denk T, Dones L, Dyudina U, Evans MW, Fussner S, Glese B, Grazier K, Helfenstein P, Ingersoll AP, Jacobson RA, Johnson TV, McEwen A, Murray CD, Neukum G, Owen WM, Perry J, Roatsch T, Spitale J, Squyres S, Thomas P, Tiscareno M, Turtle EP, Vasavada AR, Veverka J, Wagner R, West R (2005) Imaging of Titan from the Cassini spacecraft. Nature 434:159–168

Radebaugh J, Lorenz RD, Lunine JI, Wall SD, Boubin G, Reffet E, Kirk RL, Lopes RM, Stofan ER, Soderblom L, Allison M, Janssen M, Paillou P, Callahan P, Spencer C (2008) the Cassini radar team: dunes on Titan observed by Cassini radar. Icarus 194:690–703

Rannou P, Hourdin F, McKay CP, Luz D (2004) A coupled dynamics-microphysics model of Titan's atmosphere. Icarus 170:443–479

Rannou P, Montmessin F, Hourdin F, Lebonnois S (2006) The latitudinal distribution of clouds on Titan. Science 311:201–205

Richardson MI, Toigo AD, Newman CE (2007) PlanetWRF: a general purpose, local to global numerical model for planetary atmospheric and climate dynamics. J Geophys Res 112:E09001

Rodriguez S, Le Mouélic S, Rannou P, Tobie G, Baines KH, Barnes JW, Griffith CA, Hirtzig M, Pitman KM, Sotin C, Brown RH, Buratti BJ, Clark RN, Nicholson PD (2009) Clouds revealing Titan's global climatology. Nature (in press)

Roe HG, de Pater I, Macintosh A, McKay CP (2002) Titan's clouds from Gemini and Keck adaptive optics imaging. Astrophys J 581: 1399–1406

Roe HG, Brown ME, Schaller EL, Bouchez AH, Trujillo CA (2005) Geographic control of Titan's mid-latitude clouds. Science 310: 477–479

Roman MT, West RA, Banfield DJ, Gierasch PJ, Achterberg RK, Nixon CA, Thomas PC (2009) Determining a tilt in Titan's north–south albedo asymmetry from Cassini images. Icarus (submitted)

Schaller EL, Brown ME, Roe HG, Bouchez AH (2006a) A large cloud outburst at Titan's south pole. Icarus 182:224–229

Schaller EL, Brown ME, Roe HG, Bouchez AH, Trujillo CA (2006b) Dissipation of Titan's south polar clouds. Icarus 184:517–523

Schneider T (2006) The general circulation of the atmosphere. Ann Rev Earth Planet Sci 34:65–688

Sicardy B et al (1999) The structure of Titan's stratosphere from the 28 Sgr occultation. Icarus 142:357–390

Sicardy B, Colas F, Widemann T et al (2006) The two Titan stellar occultations of 14 November 2003. J Geophys Res 111:E11S91. doi:10.1029/2005JE002624

Sromovsky LA, Suomi VE, Pollack JB, Krauss RJ, Limaye SS, Owen T, Revercomb HE, Sagan C (1981) Implications of Titan's north–south brightness asymmetry. Nature 292:698–702

Stiles BW, Kirk RL, Lorenz RD, Hensley S, Lee E, Ostro SJ, Allison MD, Callahan PS, Gim Y, Iess L, Persi del Marmo P, Hamilton G, Johnson WTK, West RD, the Cassini RADAR Team (2008) Determining Titan's spin state from Cassini RADAR images. Astron J 135:1669–1680

Stofan ER, Elachi C, Lunine JI, Lorenz RD, Stiles B, Mitchell KL, Ostro S, Soderblom L, Wood C, Zebker H, Wall S, Janssen M, Kirk R, Lopes R, Paganelli F, Radebaugh J, Wye L, Anderson Y, Allison M, Boehmer R, Callahan P, Encrenaz P, Flamini E, Francescetti G, Gim Y, Hamilton G, Hensley S, Johnson WTK, Kelleher K, Muhleman D, Paillou P, Picardi G, Posa F, Roth L, Seu R, Shaffer S, Vetrella S, West R (2007) The lakes of Titan. Nature 445:61–64

Strobel DF (2006) Gravitational tidal waves in Titan's upper atmosphere. Icarus 182:251–258

Strobel DF, Atreya SK, Bézard B, Ferri F, Flasar FM, Fulchignoni M, Lellouch E, Müller-Wodarg I (2009) Atmospheric composition and structure. In: Brown RH, Lebreton J-P, Waite JH (eds) Titan after Cassini-Huygens. Springer [AU19]

Teanby NA, Irwin PGJ, de Kok R, Nixon CA, Coustenis A, Bézard B, Calcutt SB, Bowles NE, Flasar FM, Fletcher L, Howett C, Taylor FW (2007) Latitudinal variations of HCN, $HC_3N$ and $C_2N_2$ in Titan's stratosphere derived from Cassini CIRS data. Icarus 181: 364–384

Teanby NA, de Kok R, Irwin PGJ, Osprey S, Vinatier S, Gierasch PJ, Read PL, Flasar FM, Conrath BJ, Achterberg RK, Bézard B, Nixon CA, Calcutt S (2008) Titan's winter polar vortex structure revealed by chemical tracers. J Geophys Res 113:E12003

Teanby NA, Irwin PGJ, de Kok R, Nixon CA (2009) Dynamical implications of seasonal and spatial variations in Titan's stratospheric composition. Phil Trans Roy Soc London 367:697–711

Tokano T (2005) Meteorological assessment of the surface temperatures on Titan: constraints on the surface type. Icarus 173:222–242

Tokano T (2007) Near-surface winds at the Huygens site on Titan: interpretation by means of a general circulation model. Planet Space Sci 55:1990–2009

Tokano T (2008a) Dune-forming winds on Titan and the influence of topography. Icarus 194:243–262

Tokano T (2008b) The dynamics of Titan's troposphere. Phil Trans Roy Soc London 367:633–648

Tokano T, Neubauer FM (2002) Tidal winds on Titan caused by Saturn. Icarus 158:499–515

Tokano T, Neubauer FM (2005) Wind-induced seasonal angular momentum exchange at Titan's surface and its influence on Titan's length-of-day. Geophys Res Lett 32:L24203

Tokano T, Neubauer FM, Laube M, McKay CP (1999) Seasonal variation of Titan's atmospheric structure simulated by a general circulation model. Planet Space Sci 47:493–520

Tokano T, Neubauer FM, Laube M, McKay CP (2001) Three-dimensional modeling of the tropospheric methane cycle on Titan. Icarus 153:130–147

Tokano T, Ferri F, Colombatti G, Mäkinen T, Fulchignoni M (2006) Titan's planetary boundary layer structure at the Huygens landing site. J Geophys Res 111:E08007

Tomasko MG, Smith PH (1982) Photometry and Polarimetry of Titan: Pioneer 11 observations and their implications for aerosol properties. Icarus 51:65–95

Tomasko MG, Archinal B, Becker T, Bézard B, Bushroe M, Combes M, Cook D, Coustenis A, de Bergh C, Dafoe C, Doose LE, Douté S, Eibl A, Engel S, Gliem F, Grieger B, Holso K, Howington-Kraus E, Karkoschka E, Keller HU, Kirk R, Kramm R, Küppers M, Lanagan P, Lellouch E, Lemmon M, Lunine J, McFarlane E, Moores J, Prout GM, Rizk B, Rosiek M, Rueffer P, Schröder SE, Schmitt B, See C, Smith P, Soderblom L, Thomas N, West R (2005) Rain,

Uncorrected Proof

winds and haze during the Huygens probe's descent to Titan's surface. Nature 438:765–778

Tomasko MG, Bézard B, Doose L, Engel S, Karkoschka E, Vinatier S (2008) Heat balance in Titan's atmosphere. Planet Space Sci 56: 648–659

Toon OB, McKay CP, Courtin R, Ackerman TP (1988) Methane rain on Titan. Icarus 75:255–284

Turtle EP, Perry JE, McEwen AS, DelGenio AD, Barbara J, West RA, Fussner S, Dawson DD, Porco CC (2008) Cassini Imaging of Titan's high-latitude lakes, clouds, and south-polar surface changes. Nature (submitted)

Vander Auwera J, Moazzen-Ahmadi N, Flaud J-M (2008) Towards an accurate database for the 12 mm region of the ethane spectrum. Astrophys J 662:750–757. doi:10.1086/515567

Walterscheid RL, Schubert G (2006) A tidal explanation for the Titan haze layers. Icarus 183:471–478

Williams GP (1988) The dynamical range of global circulations–II. Climate Dynamics 3:45–84

Witasse O, Lebreton JP, Bird MK, Dutta-Roy R, Folkner, WM, Preston RA, Asmar SW, Gurvits LI, Pogrebenko SV, Avruch IM, Campbell RM, Bignall HE, Garrett MA, van Langevelde HJ, Parsley SM, Reynolds C, Szomoru A, Reynolds JE, Phillips CJ, Sault RJ, Tzioumis AK, Ghigo F, Langston G, Brisken W, Romney JD, Mujunen A, Ritakari J, Tingay SJ, Dodson RG, van't Klooster CGM, Blancquaert T, Coustenis A, Gendron E, Sicardy B, Hirtzig M, Luz D, Negrao A, Kostiuk T, Livengood TA, Hartung M, de Pater I, Adamkovics M, Lorenz RD, Roe H, Schaller E, Brown M, Bouchez AH, Trujillo CA, Buratti BJ, Caillault L, Magin T, Bourdon A, Laux C (2006) Overview of the coordinated ground-based observations of Titan during the Huygens mission. J Geophys Res 111:E07S01. doi:10.1029/2005JE002640

Zhu X (2006) Maintenance of equatorial superrotation in the atmospheres of Venus and Titan. Planet Space Sci 54:761–773

Zhu X, Strobel DF (2005) On the maintenance of thermal wind balance and equatorial superrotation in Titan's stratosphere. Icarus 176:331–350

Uncorrected Proof

## Author Queries:

AU1: 'Flasar and Achterberg (2008)' is cited in text but not given in the reference list. Please provide details in the list or delete the citation from the text.
AU2: 'Smith et al. 1981' is cited in text but not given in the reference list. Please provide details in the list or delete the citation from the text.
AU3: 'Yelle et al. (1997)' is cited in text but not given in the reference list. Please provide details in the list or delete the citation from the text.
AU4: The citation 'Colombatti et al. 2006' (original) has been changed to 'Colombatti et al., 2008'. Please check if appropriate.
AU5: The citation 'Dutta-Roy et al. 2004' (original) has been changed to 'Dutta-Roy and Bird, 2004'. Please check if appropriate.
AU6: Please provide author initials for "Gurvits et al. personal communication, 2009".
AU7: Please specify if the year is "2008a" or "2008b" in Achterberg et al. 2008 as per reference list.
AU8: Reference citations: "Teanby et al. 2005; Coustenis et al. 2007; Coustenis and Bézard 1995; and Vinatier et al. 2007" are cited in text but not given in the reference list. Please provide details in the list or delete the citations from the text.
AU9: The citation 'Vander Auwera et al. 2007' (original) has been changed to 'Vander Auwera et al., 2008'. Please check if appropriate.
AU10: Reference citations: "Griffith et al. 2006; Samuelson et al. 1997, 2007; Khanna 2005; Coustenis et al. 1999" are cited in text but not given in the reference list. Please provide details in the list or delete the citations from the text.
AU11: Please check and update the citation of "Section 13.3.4" here since there is no such section in this chapter.
AU12: 'Teanby et al. 2006' is cited in text but not given in the reference list. Please provide details in the list or delete the citation from the text.
AU13: Following references are not cited in text: Flasar (1983) Lellouch et al. (1989)
AU14: Please update the following references: Achterberg et al. (2008b); Rodriguez et al. (2009).
AU15: Please provide date of access of website for this reference
AU16: Please update Friedson et al. (2008).
AU17: Please provide provide location detail for Lorenz et al. (2009).
AU18: Please check and update the following references: Pentaedo et al. (2008); Roman et al. (2009); Turtle et al. (2008).
AU19: Please provide place of publication for Strobel et al. (2009).

Uncorrected Proof